ÉCOLE DE TECHNOLOGIE SUPÉRIEURE
UNIVERSITÉ DU QUÉBEC

THESIS PRESENTED TO
ÉCOLE DE TECHNOLOGIE SUPÉRIEURE

IN PARTIAL FULFILLMENT OF THE REQUIREMENTS FOR
THE DEGREE OF MASTER OF ENGINEERING
M.Eng.

BY
NJOYA MOTAPON, Souleman

A GENERIC FUEL CELL MODEL AND EXPERIMENTAL VALIDATION

MONTREAL, SEPTEMBER 11 2008

THIS THESIS HAS BEEN EVALUATED

BY THE FOLLOWING BOARD OF EXAMINERS

- M. Louis-A. Dessaint, Thesis Supervisor
  Département de génie électrique de l'École de technologie supérieure

- M. Kamal Al-Haddad, President of the Board of Examiners
  Département de génie électrique de l'École de technologie supérieure

- M. Guy Olivier, professeur
  Département de génie électrique et de génie informatique de l'École Polytechnique de Montréal

THIS THESIS HAS BEEN PRESENTED AND DEFENDED

BEFORE A BOARD OF EXAMINERS AND PUBLIC

SEPTEMBER 10 2008

AT ÉCOLE DE TECHNOLOGIE SUPÉRIEURE

A GENERIC FUEL CELL MODEL AND EXPERIMENTAL VALIDATION

Njoya Motapon Souleman

ABSTRACT

Fuel cells offer clean, quiet and efficient electrical energy. Environmental issues regarding the emissions of green house gases have propelled the use of fuel cells in applications such as automotive, mobile and power generation systems.

These fuel cells generate unregulated DC voltage and are usually connected to a power system through DC-DC converters. The design and simulation of such converters or the whole power system require an accurate model of fuel cells. Many publications on fuel cell modeling have been reported in the previous years, but most of the proposed fuel cells models are obtained empirically or through experiments on actual fuel cells. These models are only valid for particular fuel cells and can not be generalized. This does not facilitate the simulation and the design of fuel cells power systems, especially when the user does not have the fuel cells at hands.

In this project, a new approach of fuel cell modeling is proposed, an approach where the fuel cells model is obtained from data from fuel cells datasheets which are provided by stack manufacturers and publicly available. The model is a generic model and able to emulate the behavior of any fuel cell types fed with hydrogen and air.

The model is validated through comparison with real datasheet performance and with experimental data from an actual fuel cell stack. The datasheet of a 6kW-45V proton exchange membrane fuel cell (PEMFC) from NedStack is considered for the study and experimental tests are performed on a 500W-48V PEMFC (EPAC-500). The simulations results obtained are close to the expected results with an error in the range of $\pm 1\%$, that for both steady and transient states and at any condition of operation, provided a controlled stack internal humidity. However, the model gives an error of 1% for every 9% increase in air pressure and an error of 3% for a 15% decrease in temperature due to the effect of humidity.

This model is integrated in SimPowerSystems (SPS) and made available to SPS users. A fuel cell vehicle demonstration (FCV demo) is presented to point out the advantages of the proposed model in the simulation of fuel cell power systems and to show how the fuel cell model inter-connects with other electrical systems. The vehicle is modeled with the same characteristics as the Honda FCX-Clarity developed by Honda. The performances of the fuel cell model and the vehicle are close to their real values in terms of fuel consumption, maximum speed and acceleration. This confirms the validity of the FCV demo.

The FCV demo is a typical application of fuel cells and can be used as a perfect starting point on the design and simulation of fuel cell power systems.

MODÈLE GÉNÉRIQUE D'UNE PILE À COMBUSTIBLE ET VALIDATION EXPÉRIMENTALE

Njoya Motapon Souleman

RÉSUMÉ

Les piles à combustibles font partie des sources d'énergie renouvelables offrant une énergie électrique propre, silencieuse et avec un rendement élevé. Elles prennent en entrée l'hydrogène et l'air et les convertissent en énergie électrique à travers des réactions électrochimiques. Cette conversion ne génère que de l'eau et la chaleur.

Les problèmes environnementaux crées par la croissance en émissions des gaz à effet de serre ont augmenté l'utilisation de ces piles dans les domaines tels que: les transports, les portables et la génération de l'énergie électrique.

Ces piles produisent une tension électrique qui varie de façon non linéaire avec le courant et elles sont le plus souvent connectées avec d'autres systèmes électriques à travers des convertisseurs CC-CC. Dans la conception et la simulation des ces convertisseurs ou même de tout le système électrique, un modèle précis de ces piles est nécessaire. Plusieurs articles concernant la modélisation des piles à combustibles ont été publiés dans les années antérieures, mais la majorité des modèles présentés sont obtenus de façon empirique ou à travers des expériences sur des vraies piles. Ces modèles sont seulement valides pour une pile en particulier et ne peuvent être généralisés. Cela rend difficile la conception et la simulation des systèmes électriques basés sur les piles à combustible, surtout lorsque l'utilisateur ne dispose pas d'une vraie pile.

Dans ce projet, une nouvelle approche de modélisation est proposée, une approche où le modèle de pile est obtenu à l'aide des données des fiches techniques des manufacturiers et qui sont disponibles aux usagers. Le model est générique et capable de représenter le comportement de n'importe quel type de pile alimentée par l'hydrogène et l'air.

Le modèle est validé par des comparaisons avec les données des fiches techniques et avec les résultats des tests sur une vraie pile. Une fiche technique d'une pile de 6kW-45V à membrane échangeuse de protons (PEMFC) de NedStack est considérée pour l'étude et les expériences sont performées sur une pile de 500W-48V (EPAC-500). Les résultats de simulation sont très proches des résultats attendus avec juste une erreur (entre la tension donnée par le modèle et la tension réelle) qui varie entre ±1%, ceci tant en régime permanent qu'en régime transitoire et à n'importe quelle condition d'opération. Ce résultat est valide si l'humidité à l'intérieur de la pile est bien contrôlée. Cependant le modèle produit une erreur de 1% lorsque la pression d'air augmente de 9% et une erreur d'environs 3% lorsque la température décroît de 15% sous l'effet de l'humidité.

Le modèle proposé est intégré dans SimPowerSystems (SPS) et rendu disponible pour les usagers du SPS. Un modèle de démonstration d'un véhicule électrique basé sur une pile à combustible est présenté pour faire ressortir les avantages du modèle proposé dans la simulation des systèmes électriques basés sur les piles à combustibles et pour aussi montrer comment la pile interagit avec d'autres éléments électriques. Ce véhicule est modélisé avec les mêmes caractéristiques que le nouveau véhicule développé par Honda (la FCX-Clarity-2008). Les performances du modèle de pile et du véhicule sont similaires à la réalité en termes de consommation en hydrogène, vitesse maximale et accélération. Ce qui confirme la validité du modèle du véhicule.

Le modèle du véhicule est une application claire des piles à combustible et peut être utilisé comme un point de départ dans la conception et la simulation des systèmes électriques basés sur les piles à combustibles.

ACKNOWLEDGMENTS

This report presents my research work carried out at École de technologie supérieure during my M.Eng. programme (From January 2007 to August 2008).

This project was presented to me by M. Louis-A. Dessaint in the winter of 2007 and I was excited to participate in this project as it was one of the research fields I was deeply interested in pursuing. I have previously worked in this field, as a graduate from Aalborg University, Denmark in 2005, my M.Sc. thesis was on the fuel cell DC-DC converter; moreover, after graduation I was hired as a research assistant to develop a direct methanol fuel DC-DC converter for the American Power Conversion (APC) in Denmark. This project has proven to be a continuation of my previous research works but with more emphasis on the fuel cell itself, rather than exclusively on converters, which makes it very interesting. Having completed this latest research project, I am confident in my understanding of the overall system.

I would like to thank professor Dessaint for his trust in me in undertaking this project and for his financial assistance, which enabled me to focus effectively on my research activities. Moreover, his constructive guidance and support throughout the project period was very much appreciated.

I would like to thank also Olivier Tremblay for his time and support. He was always there when I needed his experience and advice throughout the project period.

My sincere thanks goes to the technical staffs of Institut de recherche sur l'hydrogène in Trois-Rivières for allowing me to perform experimental tests on their fuel cell stacks. This was crucial in the validation of the proposed model. In particular, I would like to thank professor Kodjo Agbossou, Julien Ramousse and Bruno Gagnon-Vivier for their assistance and advice during the experimental tests.

I would also like to thank my family, for their support and encouragement since I left home. They know how hard it is to live far from home and they always manage to make me feel like they are right by my side.

Finally, with all my heart, I would like to express my gratitude to my girlfriend Amy, for her time reviewing this report, her support and most importantly her love. Her great advice was very much appreciated.

CONTENTS

Page

LIST OF TABLES

LIST OF FIGURES

NOMENCLATURE

A	Tafel slope (V)
B	Mass transport constant (V)
c_{O_2}	oxygen concentration (mol/m^3)
C_p	Heat capacity of the cell (J/kg K)
D_{ij}^{eff}	Effective binary diffusivity (m^2/s)
E	Thermodynamic voltage (V)
E_n	Nernst voltage (V)
E_{oc}	Open circuit voltage (V)
F	Faraday constant (A s/mol)
h	Planck's constant (J s)
i_{fc}	Cell current (A)
i_l	Limiting current density (A/m^2)
i_0	exchange current (A)
J_i	Molar flux of species i (mol/m^2 s)
k	Boltzmann's constant (J/K)
K_{valve}^{i}	Valve constant associated to species i (mol/atm s)
M_p	Mass of the cell (kg)
m, n	Concentration losses constant
N	Number of cells in series
n_i	Flow rate of species i (mol/s)
P	Cell output power (kW)

P_i	Partial pressure of species i (atm)
P_t	Total pressure (atm)
q_e	Electrochemical reaction heat (J/m^3)
Q_i	Total heat generated due to species i (J)
r	Cell resistance (Ω)
R	Ideal gas constant (J/mol K)
R_{ohm}	Stack resistance (Ω)
T	Cell temperature (^oK)
T_d	Cell response time (s)
U_{f_i}	Utilization of species i (%)
V	Cell voltage (V)
V_{air}	Air flow rate (sl/min)
V_{act}	Activation voltage (V)
V_c	Volume of the cathode/anode(m^3)
V_{conc}	Concentration voltage(V)
V_e	Cell volume (m^3)
V_{fc}	Stack voltage (V)
V_r	Resistive voltage(V)
V_u	Voltage undershoot (V)
x_i	Mole fraction of species i
z	Number of moving electrons
α	Exchange coefficient

ξ_i	Activation losses constants
Δg	Reaction gibbs free energy (J)
ΔG	size of the activation barrier (J/mol)
Δh	Reaction enthalpy (J)
Δs	Reaction entropy (J/K)
η	Cell efficiency (%)
AFC	Alkaline Fuel Cell
CC	Courant continu
CHP	Combined Heat and Power
DC	Direct current
DMFC	Direct Methanol Fuel Cell
FCV	Fuel Cell Vehicle
LHV	Low Heating Value
MCFC	Molten Carbonate Fuel Cell
PAFC	Phosphoric Acid Fuel Cell
PEMFC	Proton Exchange Membrane Fuel Cell
PI	Proportionnal-Integral regulator
SPS	SimPowerSystems
SOFC	Solid Oxide Fuel Cell

INTRODUCTION

Over the last decade, there have been some growing concerns regarding the emission of greenhouse gases and the shrinking of fossil fuel reserves which have made fuel cell energy sources very attractive. This is mainly due to their high reliability, low emission of pollutants and little maintenance (Xin and Khambadkone, 2003).

Fuel cells are electrochemical devices that convert chemical energy from an electrolytic reaction directly to electrical energy, rejecting only heat and water. A cell consists of an electrolyte in contact with two porous electrodes (the anode and the cathode) on either side. Hydrogen gas passes over the anode, and with the help of a catalyst, separates into electrons and hydrogen ions. These ions flow to the cathode through the electrolyte while the electrons flow through an external circuit (electricity is generated). At the cathode, the hydrogen ions combine with oxygen (from air) to form water. This is shown in figure 1.

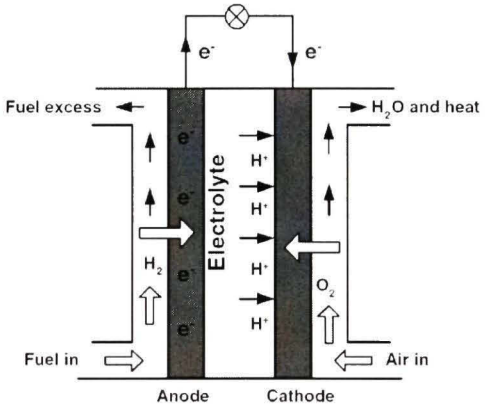

Figure 1 ***Fuel cell operating principle.***
(From IEEE transaction, Xin et al., 2005)

Source: Kong Xin, Ashwin M. Khambadkone, Soy Kee Thum, *A hybrid model with combined steady state and dynamic characteristic of PEMFC fuel cell stack*, p. 1618. IEEE transaction.

It can be noted from figure 1 that the resulting current flows in the opposite direction (opposite to the conventional direction). This can be explained from the fact that in any conductive materials, the flow of protons or holes constitutes the electric current.

The nominal voltage produced from one cell is about 0.7 V. To obtain higher voltages, several cells are placed in series to form a fuel cell stack.

Depending on their operating temperature and the type of electrolyte used, there exist different kinds of fuel cells. Types of fuel cells along with their mobile ion, operating temperature and applications are summarized in table I.

Table I

Fuel cell types

(From Larminie and Dicks, 2003)

Fuel cell type	Mobile ion	Operating temperature	Applications and notes
Alkaline (AFC)	OH^-	50–200°C	Used in space vehicles, e.g. Apollo, Shuttle.
Proton exchange membrane (PEMFC)	H^+	30–100°C	Vehicles and mobile applications, and for lower power CHP systems
Direct methanol (DMFC)	H^+	20–90°C	Suitable for portable electronic systems of low power, running for long times
Phosphoric acid (PAFC)	H^+	~220°C	Large numbers of 200-kW CHP systems in use.
Molten carbonate (MCFC)	CO_3^{2-}	~650°C	Suitable for medium- to large-scale CHP systems, up to MW capacity
Solid oxide (SOFC)	O^{2-}	500–1000°C	Suitable for all sizes of CHP systems, 2 kW to multi-MW.

Source: James Larminie, Andrew Dicks, *Fuel cell systems explained*, 2nd edition, John Wiley and Sons Ltd.

Areas of application of fuel cells include: distributed power generation, back-up power generation, automotive and other consumer applications including cellular phones, PDAs (Personal Digital Assistants) and laptops.

Recently, Honda (http://world.honda.com/FuelCell) made available to some customers, a new fuel cell vehicle (FCV), the Honda FCX clarity, which makes the use of fuel cells a commercial reality.

In spite of being a clean source of energy, fuel cells are only capable of producing unregulated dc voltage, hence the need for power converters to interface the driven load. An accurate model of fuel cells is needed to observe their dynamic and steady state performances necessary for the design, control and simulation of such converters. A lot of research work has been done in fuel cell modeling. Most of the models found in the literature are based on the chemical and thermodynamic aspects of the fuel cell. These models can not be easily added to electrical simulations programs. Other models represent the fuel cell by electrical circuit elements. The later models do not include the fuel cell thermodynamics, but could be used in the simulation of fuel cell power systems. In both approaches of modeling, the model parameters are obtained either empirically or by performing some tests on the real fuel cell.

The objectives of this project are:

a. To develop a fuel cell model
b. To validate this model with experimental data obtained on real fuel cells

In addition, model parameters will have to be derived directly from fuel cells manufacturer's datasheets.

This report is organized into the following sections:

a. Chapter 1: Presents briefly a literature survey of previous researches regarding fuel cell modeling.
b. Chapter 2: The proposed model is developed and implemented in SPS (SimPowerSystems) with the objective of minimum input parameters

requirement and higher accuracy.

c. Chapter 3: Deals with the validation of the model and presents the correlation between the simulation results and the experimental results obtained from a real setup.

d. Chapter 4: Presents the performance of the model in a fuel cell vehicle (FCV) demonstration in SPS.

The final section concludes with a synopsis of the report and identifies future works to be done for model improvement.

CHAPTER 1

LITERATURE REVIEW

Several types of fuel cells models exist in articles and books. These models can be classified into three categories which are: chemical or mechanical models, look-up table or curve fitting models and electrical models.

1.1 Chemical or mechanical models

These models include complex chemical and thermodynamic phenomenon such as the mass transport, heat transfer and diffusion of species inside the cell. Based on the level of complexity, they can be:

a. Multi-dimensional: Usually used to design fuel cell components and to predict accurately the internal state of cells parameters such as the membrane water content, reactant concentration, catalyst utilization and membrane degradation (O'Hayre *et al.*, 2006). They involve the use of partial differential equations. CFD (Computational fluid dynamics) models developed by Liu and Zhou (2003) fall into this category. These models require longer simulation time and excessive amount of parameters (flow channel width, thickness of the electrolyte, porosity of electrodes, cell volume) which are difficult to determine. As the goal of this project is to emulate the behavior of real fuel cells and not to design them, these models are not pertinent for this study.

b. One-dimensional: Widely found in the literature, they represent pressure and temperature dynamics by first order differential equations. Models developed by researchers such as Yu *et al.* (2006), Pukruspan *et al.* (2004), Uzunoglu and Alam (2006), Sedghisigarchi and Feliachi (2004), Zhu and Tomsovic (2002) are all one-dimensional. First, reactants partial pressures and cell temperature are obtained from mass and energy conservation principles respectively. Then, the

reversible voltage is obtained from the Nernst equation. Finally, the actual cell voltage is determined considering the irreversible losses which include the activation, ohmic and concentration losses. These models are extended to include the diffusion process by some researchers such as Kopasakis *et al.* (2006) and Wang *et al.* (2005). Table II shows equations involved in this approach, definitions of parameters can be found on the nomenclature section of the report.

Table II

Fuel cell modeling equations

Nersnt equation	$E_n = 1.229 + (\mathrm{T}-298)\frac{-44.43}{zF} + \frac{RT}{zF}\ln\left(P_{H_2}P_{O_2}^{\frac{1}{2}}\right)$
Mass conservation	$\frac{dP_i}{dt} = \frac{RT}{V_c}(n_i^{in} \pm n_i^r - n_i^{out}),\ n_i^{out} = K_{valve}^i P_i$
Energy conservation	$M_p C_p \frac{dT}{dt} = q_e V_e + \sum Q_i$
Diffusion process	$\frac{dx_i}{dz} = \frac{RT}{P_t}\sum_{j \neq i}\frac{x_i J_j - x_j J_i}{D_{ij}^{eff}}$
Actual cell voltage	$V = E_n - V_{act} - V_r - V_{conc}$ $V_{act} = A\ln\left(\frac{i_{fc}}{i_0}\right)$ $V_{act} = \xi_1 + \xi_2 T + \xi_3 T\ln(c_{O_2}) + \xi_4\ln(i_{fc})$ $V_r = r i_{fc}$ $V_{conc} = -B\ln\left(1 - \frac{i_{fc}}{i_l}\right),\ V_{conc} = m e^{n i_{fc}}$

Recently the EUtech Scientific Engineering GmbH (www.eutech-scientific.de) has developed a fuel cell systems library (FClib) containing a fuel cell model which is based on this approach.

Others researchers such as Larminie and Dicks (2003), Wingelaar *et al.* (2005), Tirnovan *et al.* (2006) and Pasricha *et al.* (2007) use a steady state model where the reversible voltage is assumed to be constant.

In all one-dimensional models, the procedure to determine model parameters is similar. First, experiments to obtain polarization curves (shown in figure 2) at different pressures and temperatures are made on the real fuel cell. Then, parameters (such as A, B, i_o, ξ_i, m and n) are determined by curve fitting techniques (Pukruspan *et al.*, 2004). This means the model is only valid for that particular fuel cell and the procedure to obtain parameters have to be repeated for a different fuel cell.

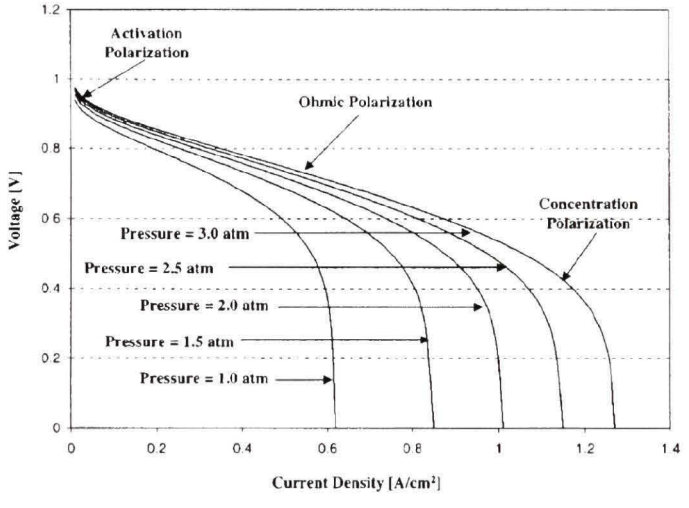

Figure 2 ***Fuel cell polarization curves.***
(From ASME transaction, Boettner et al., 2002)

Source: Daisie D. Boettner, Gino Paganelli,Yann G. Guezennec, Giorgio Rizzoni and Michael J. Moran, *Proton exchange membrane fuel cell system model for automotive vehicle simulation and control*, p. 21.Transactions of the ASME. Vol. 124.

1.2 Look-up table or curve fitting models

These models are usually used to represent fuel cells polarization curve in steady state and at nominal condition of operation. The polarization curve is input to the model in tabular form.

For a given input current, the output voltage is estimated by interpolation (linear, cubic or spline). Kim *et al.* (2005), Acharya *et al.* (2004) and Buchholz and Krebs (2007) use a linear, cubic and cubic spline interpolation method respectively. The effect of pressure, temperature and flow rate on the cell performance cannot be observed and the user has to perform large data entry prior to simulation.

1.3 Electrical models

In this approach, fuel cells are represented by equivalent electrical circuits. These models are used for both steady and dynamic states assuming a constant condition of operation. Different configurations (shown in figure 3) are reviewed by Runtz and Lyster (2005).

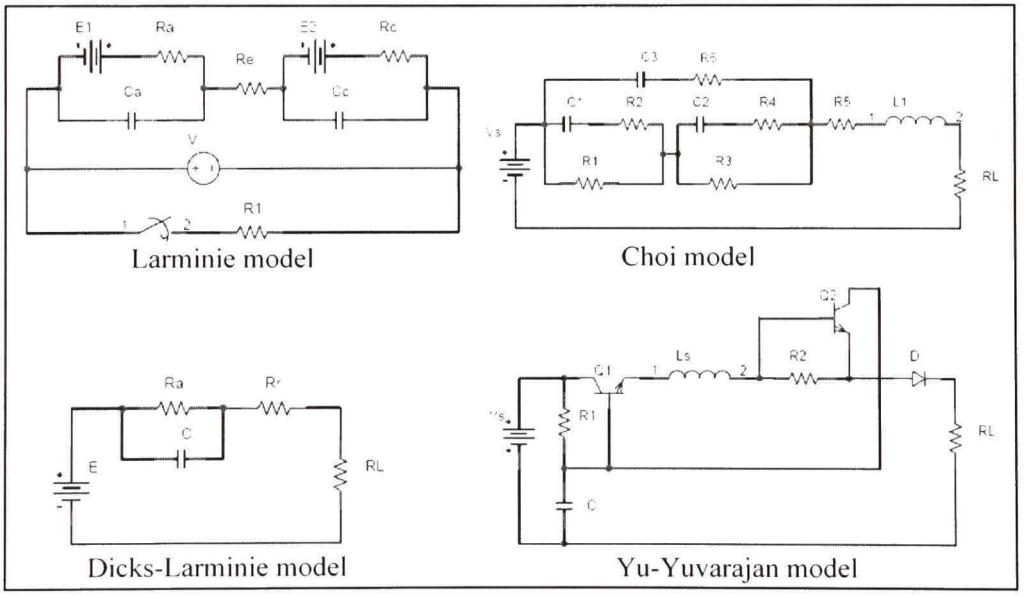

Figure 3 ***Fuel cell electrical models.***
(From IEEE transaction, Runtz and Lyster, 2005)

Source: K. J. Runtz, M. D. Lyster, *Fuel cell equivalent circuit models for passive mode testing and dynamic mode design*, p. 794 - 797. IEEE transaction.

In figure 3, models developed by Larminie and Choi use capacitors, ideal dc voltage and resistors to represent cell dynamics, the reversible voltage and cell resistances respectively. A more complex model developed by Yu and Yuvarajan is also shown where an inductor and transistors are added to represent the effect of compressor delays on the cell performance.

Again it is not possible to observe the effect of pressure, temperature and flow rate. Experimental tests such as the current interrupt, impedance spectroscopy or frequency response tests are required to obtain models parameters (cell resistances, response times, no-load voltage).

From the literature review above, it is clear that, at least the one-dimensional, chemical model should be used to predict the behavior of fuel cells at any condition of operation. But it requires experiments to be made on each fuel cell (or stack) under study to determine model parameters. A more generic fuel cell model is needed; a model that will emulate the behavior of any type of fuel cells with no experimental tests (or at least one test at nominal condition if no data is available).

The next section presents the development of the proposed model, the model input parameters are obtained directly from stack manufacturer's datasheets.

CHAPTER 2

FUEL CELL MODELING

2.1 Introduction

This chapter presents in a more detailed manner the proposed fuel cell model. At first the modeling equations which involve the thermodynamic generated voltage, fuel cell losses, dynamics and efficiency are derived. Then, the cell actual voltage is deduced and two models (simplified and detailed) are proposed and implemented in Matlab/SimPowerSystems (SPS).

The simplified model is used for the simulation of fuel cells at nominal condition whereas the detailed one is used for all conditions of operation. In both models, the input parameters are extracted from fuel cells datasheets.

2.2 Model assumptions

The following assumptions are made for the model:

a. The gases are ideal
b. The stack is fed with hydrogen and air
c. The temperature at the cathode and anode is considered stable and equal to the stack temperature
d. The ratio of pressures between the interior and exterior of each flow channel is large enough to consider that the orifice is choked
e. Pressures drops across flow channels are negligible
f. The cell voltage drops are due to reaction kinetics and charge transport as most fuel cells do not operate in the mass transport region
g. The cell resistance is constant at any condition of operation (information on the type or dimension of electrodes and electrolyte is not generally provided on fuel cell datasheets)

2.3 Fuel cell modeling equations

2.3.1 Fuel cell reversible (thermodynamic) voltage

The reversible or thermodynamic voltage is the voltage generated by the fuel cell at equilibrium due to electrochemical reactions at the electrodes.

Table III shows electrochemical reactions for common fuel cells type fed with hydrogen and air. The overall reaction is given by:

$$H_2 + \frac{1}{2}O_2 \rightarrow H_2O \tag{2-1}$$

Table III

Cell's electrodes reactions

Cell types	Electrode reactions
Alkaline Fuel Cell (AFC)	$Anode: H_2 + 2(OH)^- \rightarrow 2H_2O + 2e^-$ $Cathode: \frac{1}{2}O_2 + H_2O + 2e^- \rightarrow 2(OH)$
Proton Exchange Membrane Fuel Cell (PEMFC) and Phosphoric Acid Fuel Cell (PAFC)	$Anode: H_2 \rightarrow 2H^+ + 2e^-$ $Cathode: 2H^+ + 2e^- + \frac{1}{2}O_2 \rightarrow H_2O$
Molten Carbonate Fuel Cell (MCFC)	$Anode: \begin{cases} H_2 + CO_3^{2-} \rightarrow H_2O + CO_2 + 2e^- \\ CO + CO_3^{2-} \rightarrow 2CO_2 + 2e^- \end{cases}$ $Cathode: CO_2 + 2e^- + \frac{1}{2}O_2 \rightarrow CO_3^{2-}$
Solid Oxide Fuel Cell (SOFC)	$Anode: H_2 + O^{2-} \rightarrow H_2O + 2e^-$ $Cathode: 2e^- + \frac{1}{2}O_2 \rightarrow O^{2-}$

The energy potential (the Gibbs free energy) of this reaction is given at standard temperature and pressure by (O'Hayre *et al.*, 2006):

$$\Delta g^0 = \Delta h^0 - T_0 \Delta s^0 \tag{2-2}$$

Where Δg^0 = reaction Gibbs free energy, Δh^0 = reaction enthalpy, Δs^0 = reaction entropy and T_0 = standard temperature (298 K)

The standard-state thermodynamic voltage is given by:

$$E^0 = -\frac{\Delta g^0}{zF} \tag{2-3}$$

Where E^0 = standard thermodynamic voltage, z = number of moving electrons and F = Faraday's constant (96485 A s/mol).

At non standard-state condition, the thermodynamic voltage varies with pressure and temperature. It is given by the Nernst equation as follows:

$$E_n = \begin{cases} E^0 + (T - T_0) \cdot \dfrac{\Delta s^0}{zF} + \dfrac{RT}{zF} \ln\left(P_{H_2} P_{O_2}^{\frac{1}{2}} \right) & T \le 100^0 C \\ E^0 + (T - T_0) \cdot \dfrac{\Delta s^0}{zF} + \dfrac{RT}{zF} \ln\left(\dfrac{P_{H_2} P_{O_2}^{\frac{1}{2}}}{P_{H_2O}} \right) & T > 100^0 C \end{cases} \tag{2-4}$$

Where E_n = thermodynamic voltage at a given condition, T = Temperature of operation, R = ideal gas constant (8.3145 J/ mol K), P_i = Partial pressure of species i inside the cell.

From thermodynamic tables, E^0 and Δs^0 are determined and equation (2-4) becomes:

$$E_n = \begin{cases} 1.229 + (T - 298) \cdot \dfrac{-44.43}{zF} + \dfrac{RT}{zF} \ln\left(P_{H_2} P_{O_2}^{\frac{1}{2}} \right) & T \le 100\,^{\circ}C \\ 1.229 + (T - 298) \cdot \dfrac{-44.43}{zF} + \dfrac{RT}{zF} \ln\left(\dfrac{P_{H_2} P_{O_2}^{\frac{1}{2}}}{P_{H_2O}} \right) & T > 100\,^{\circ}C \end{cases} \quad (2\text{-}5)$$

The change in partial pressure P_i along the flow channel is determined by applying the mass conservation principle given by (Kopasakis *et al.*, 2006):

$$\frac{dP_i}{dt} = \frac{RT}{V_c}(n_i^{in} \pm n_i^r - n_i^{out}) \quad (2\text{-}6)$$

Where V_c= compartment volume, n_i^{in} and n_i^{out} are the flow rates at the inlet and outlet of species i respectively, n_i^r = rate of consumption or production of species i.

For a choked orifice flow channel, the flow rate at the outlet is given by:

$$n_i^{out} = K_{valve}^i P_i \quad (2\text{-}7)$$

Where K^i_{valve} = valve constant associated with species i.

Putting equation (2-7) in equation (2-6) , we have at steady state:

$$P_i = \frac{1}{K_{valve}^i}(n_i^{in} \pm n_i^r) \quad (2\text{-}8)$$

The steady state partial pressures of H_2, H_2O and O_2 are then given by:

$$\begin{cases} P_{H_2} = \dfrac{1}{K_{valve}^{H_2}}(n_{H_2}^{in} - n_{H_2}^{r}) \\ P_{H_2O} = \dfrac{1}{K_{valve}^{H_2O}}(n_{H_2O}^{in} + n_{H_2O}^{r}) \\ P_{O_2} = \dfrac{1}{K_{valve}^{O_2}}(n_{O_2}^{in} - n_{O_2}^{r}) \end{cases} \tag{2-9}$$

When there is no current flow, no species are consumed or produced, hence $n_i^r = 0$. Therefore, the partial pressures inside the cell and at its inlet are equal. This gives:

$$\begin{cases} P_{H_2}^{in} = \dfrac{1}{K_{valve}^{H_2}} n_{H_2}^{in} \\ P_{H_2O}^{in} = \dfrac{1}{K_{valve}^{H_2O}} n_{H_2O}^{in} \\ P_{O_2}^{in} = \dfrac{1}{K_{valve}^{O_2}} n_{O_2}^{in} \end{cases} \tag{2-10}$$

Where P_i^{in} = inlet partial pressure of species *i*.

Replacing equation (2-10) in (2-9), we have:

$$\begin{cases} P_{H_2} = \dfrac{(n_{H_2}^{in} - n_{H_2}^{r})}{n_{H_2}^{in}} P_{H_2}^{in} \\ P_{H_2O} = \dfrac{(n_{H_2O}^{in} + n_{H_2O}^{r})}{n_{H_2O}^{in}} P_{H_2O}^{in} \\ P_{O_2} = \dfrac{(n_{O_2}^{in} - n_{O_2}^{r})}{n_{O_2}^{in}} P_{O_2}^{in} \end{cases} \tag{2-11}$$

If the fuel input contains x % of hydrogen and air input contains y % of oxygen and w % of water vapor, then the partial pressures at inlet can be expressed in terms of fuel and air supply pressures as follows:

$$\begin{cases} P_{H_2}^{in} = x\%P_{fuel} \\ P_{H_2O}^{in} = w\%P_{air} \\ P_{O_2}^{in} = y\%P_{air} \end{cases} \tag{2-12}$$

Where P_{fuel} and P_{air} are the supply pressures (absolute) of fuel and air respectively.

The hydrogen and oxygen utilizations are defined as:

$$\begin{cases} U_{fH_2} = \dfrac{n_{H_2}^r}{n_{H_2}^{in}} \\ U_{fO_2} = \dfrac{n_{O_2}^r}{n_{O_2}^{in}} \end{cases} \tag{2-13}$$

From equation (2-1), we have:

$$n_{O_2}^r = \frac{1}{2}n_{H_2}^r = \frac{1}{2}n_{H_2O}^r \tag{2-14}$$

Replacing equations (2-12) to (2-14) in equation (2-11), we have:

$$\begin{cases} P_{H_2} = (1 - U_{f_{H_2}})x\%P_{fuel} \\ P_{H_2O} = (w + 2y\%U_{f_{O_2}})P_{air} \\ P_{O_2} = (1 - U_{f_{O_2}})y\%P_{air} \end{cases} \tag{2-15}$$

The hydrogen and oxygen utilizations can be expressed in terms of inlet flow rates and pressures as follows:

$$\begin{cases} U_{fH_2} = \dfrac{n_{H_2}^r}{n_{H_2}^{in}} = \dfrac{60000RTi_{fc}}{zFP_{fuel}V_{lpm(fuel)}x\%} \\ U_{fO_2} = \dfrac{n_{O_2}^r}{n_{O_2}^{in}} = \dfrac{60000RTi_{fc}}{2zFP_{air}V_{lpm(air)}y\%} \end{cases} \quad (2\text{-}16)$$

Where $V_{lpm(fuel)}$ and $V_{lpm(air)}$ are the inlet flow rate (in liter/min) of fuel and air respectively, i_{fc} = cell current.

2.3.2 Fuel cell losses

The losses considered here are activation losses (due to reaction kinetics) and resistive losses (due to charge transport). These losses are described in the following sections.

2.3.2.1 Activation losses

These losses are due to the slowness of chemical reactions at the surface of electrodes (Larminie and Dicks, 2003). They are represented by the activation voltage drop (V_{act}). The region on the polarization curve affected by these losses is called the activation region.

For a PEMFC, at the cathode, the oxygen reduction and the water oxidation occur due to excess and lack of electrons on the electrode surface respectively (Larminie and Dicks, 2003). At no current, the following reactions are taking place:

$$\begin{cases} 2H^+ + \frac{1}{2}O_2 + 2e^- \rightarrow H_2O \\ 2H^+ + \frac{1}{2}O_2 + 2e^- \leftarrow H_2O \end{cases} \quad (2\text{-}17)$$

At equilibrium, we have:

$$2H^{+} + \frac{1}{2}O_2 + 2e^{-} \leftrightarrow H_2O \tag{2-18}$$

This means that there is a continual forward and reverse flow of electrons from and to the electrolyte. This movement of electrons creates a current i_0 (called the exchange current).

When the cell electrodes are connected through an external circuit, the net current flow is given by the Butler-Volmer equation as follows (O'Hayre *et al.*, 2006):

$$i_{fc} = i_0\left(e^{\frac{z\alpha FV_{act}}{RT}} - e^{-\frac{z(1-\alpha)FV_{act}}{RT}}\right) \tag{2-19}$$

Where i_0 = exchange current, α = exchange coefficient, V_{act} = activation voltage drop.

By assuming that V_{act} is large (greater than 50-100 mV at room temperature as mentioned by O'Hayre *et al.* (2006)), equation (2-19) simplifies to:

$$i_{fc} = i_0 e^{\frac{z\alpha FV_{act}}{RT}} \tag{2-20}$$

And we have:

$$V_{act} = \frac{RT}{z\alpha F}\ln\left(\frac{i_{fc}}{i_0}\right) = A\ln\left(\frac{i_{fc}}{i_0}\right) \qquad i_{fc} > i_0 \tag{2-21}$$

Where A is the slope of the Tafel curve given by:

$$A = \frac{RT}{z\alpha F} \tag{2-22}$$

Equation (2-21) is known as the Tafel equation which was verified experimentally by Tafel in 1905 (Larminie and Dicks, 2003).

The exchange current i_0 is derived from (O'Hayre *et al.*, 2006) as follows:

$$i_0 = zFc_r \frac{kT}{h} e^{\frac{-\Delta G}{RT}} \tag{2-23}$$

Where c_r = reactant concentration, k = Boltzmann's constant (1.38×10^{-23} J/^{0}K), h = Planck's constant (6.626×10^{-34} J s), ΔG = size of the activation barrier.

The reactant concentration at the electrode surface is assumed to be equal to the concentration along the flow channel, this gives:

$$c_r = c_{H_2} + c_{O_2} = \frac{P_{H_2} + P_{O_2}}{RT} \tag{2-24}$$

Where c_{H2} and c_{O2} are the hydrogen and oxygen concentration in the flow channel respectively.

Replacing equation (2-24) in (2-23), we have:

$$i_0 = \frac{zFk(P_{H_2} + P_{O_2})}{Rh} e^{\frac{-\Delta G}{RT}} \tag{2-25}$$

2.3.2.2 Resistive losses

These losses are due to resistance to charge transports. There is a voltage drop caused by the resistance of electrodes (when the electrons move from anode to cathode) and the electrolyte (when protons move from anode to cathode). This voltage drop is given by:

$$V_r = i_{fc} r \tag{2-26}$$

Where V_r = resistive voltage drop, r = cell resistance.

The region on the polarization curve affected by these losses is called the ohmic region.

2.3.3 Fuel cell dynamics

The following dynamic behaviors are considered in the model:

a. Dynamics due to the build up of charges at the electrode/electrolyte interface: At the cathode of a PEMFC for instance, there is a layer of protons and electrons on each side. This junction stores electrical energy and behaves like a capacitor. This build up of charges affects the reaction rate at the electrode, and thus the activation voltage. When there is a change in current, it takes some time (T_d), before the activation voltage drop reaches the steady state. This gives:

$$V_{act} = \frac{RT}{z\alpha F}\ln\left(\frac{i_{fc}}{i_0}\right)e^{-sT_d} = \frac{RT}{z\alpha F}\ln\left(\frac{i_{fc}}{i_0}\right)\cdot\frac{1}{sT_d+1} \tag{2-27}$$

Where T_d = cell response time.

b. Dynamics due to oxygen depletion: This is present when there is a considerable delay in the air compressor. The amount of oxygen provided at the cell input is lesser than what is required to sustain the load. Oxygen utilization increases and consequently the Nernst voltage (E_n) reduces. This creates a voltage undershoot (V_u) at the cell output. The voltage undershoot is proportional to the maximum attainable utilization which depends on the compressor delay and the current rate of increase. This effect is represented in the model by reducing the Nernst voltage by an amount proportional to the utilization when the oxygen utilization is greater than its nominal value. The Nernst voltage is modified to:

$$E_n = \begin{cases} E_n - K(U_{f_{O_2}} - U_{f_{O_2(nom)}}) & U_{f_{O_2}} > U_{f_{O_2(nom)}} \\ E_n & U_{f_{O_2}} \le U_{f_{O_2(nom)}} \end{cases} \tag{2-28}$$

Where K = voltage undershoot constant, $U_{fO2(nom)}$ = nominal oxygen utilization.

The cell dynamics are represented in figure 4.

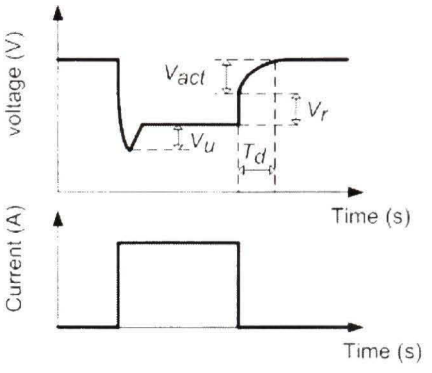

Figure 4 ***Cell dynamics.***

2.3.4 Cell efficiency

The cell efficiency is usually given with respect to the lower heating value (LHV), that's with the assumption that the water produced is in steam form. The efficiency is given by:

$$\eta = \frac{P}{n_{H_2}^{in}\Delta h°(H_2O(gas))} \times 100 = \frac{zFU_{f_{H_2}}V}{\Delta h°(H_2O(gas))} \times 100 \qquad (2\text{-}29)$$

Where P = cell output power, $\Delta h^0\ (H_2O(gas))$ = reaction enthalpy of water vapor (241.83 kJ/mol), V = cell output voltage.

2.4 Models proposed and implementation in SPS

2.4.1 Actual cell voltage

From the above discussion, the actual cell voltage can be deduced by combining the Nernst voltage, the losses and cell dynamics as follows:

$$V = E_n - A\ln\left(\frac{i_{fc}}{i_0}\right) \cdot \frac{1}{sT_d + 1} - ri_{fc} \tag{2-30}$$

For a stack with N cells in series, the stack voltage is given by:

$$V_{fc} = N \cdot \left(E_n - A\ln\left(\frac{i_{fc}}{i_0}\right) \cdot \frac{1}{sT_d + 1} - ri_{fc}\right) \tag{2-31}$$

Where V_{fc} = stack output voltage.

2.4.2 The simplified model

From equation (2-31) , we have:

$$V_{fc} = E_{oc} - NA\ln\left(\frac{i_{fc}}{i_0}\right) \cdot \frac{1}{sT_d + 1} - R_{ohm}i_{fc} \tag{2-32}$$

Where $E_{oc} = NE_n$ = open circuit voltage, $R_{ohm} = Nr$ = stack resistance.

Equation (2-32) can be represented by an equivalent circuit shown in figure 5. This circuit is a simplified model of the fuel cell stack where parameters (E_{oc}, R_{ohm}, i_o, NA) are constants.

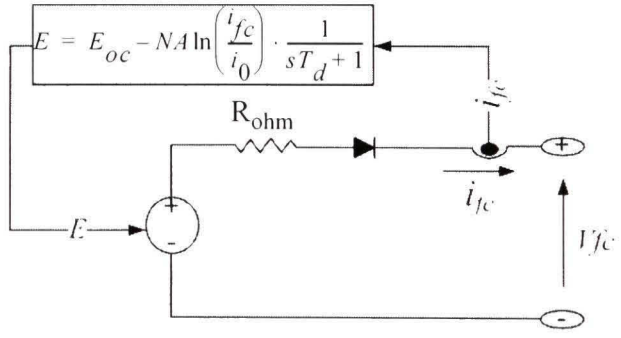

Figure 5 ***Equivalent circuit for the simplified model.***

This model represents a particular fuel cell stack operating at nominal condition of temperature and pressure. A diode is used to prevent the flow of negative current into the stack. The model is implemented in SPS exactly as in figure 5 using a controlled voltage and a $1us$ delay to break the algebraic loop (as the output voltage at time t depends on the current at the same instant). The full view of the model is shown in appendix A. The open circuit voltage is reduced exponentially to limit the output power when the current reaches its maximum value.

The data required to determine the model parameters are obtained from stack's datasheet. Generally fuel cell stack manufacturers provide data showing the stack performance at nominal condition. Data which are usually given on stack datasheets are the following (an example of a stack datasheet from NedStack is attached in appendix B):

a. Rated current, voltage and power
b. Maximum current and power
c. Number of cells
d. Stack efficiency
e. Operating temperature
f. Supply pressures of gases
g. Air and hydrogen flow rate
h. Purity of hydrogen
i. Nominal polarization curve
j. Stack response time

2.4.2.1 Data required for parameters determination

For the simplified model, four parameters (E_{oc}, R_{ohm}, i_o, NA) are to be determined, which requires at least four simultaneous equations. Two points from each region (activation and ohmic) are taken on the polarization curve as shown in figure 6.

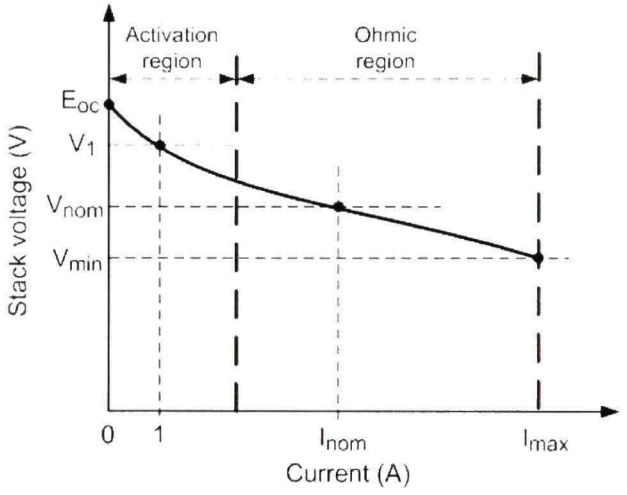

Figure 6 ***Stack polarization curve showing the required four points.***

These points correspond to the following:

a. Current and voltage at nominal operating point: (I_{nom}, V_{nom})
b. Current and voltage at maximum operating point: (I_{max}, V_{min})
c. Voltage at 0 and 1 A: (E_{oc}, V_1)

A stack response time in second (T_d) is needed if the user wishes to add the dynamic behavior of the stack.

2.4.2.2 Parameters determination

From equation (2-32) we have at steady state, the following set of equations:

$$\begin{cases} V_1 = E_{oc} + NA\ln i_0 - R_{ohm} \\ V_{nom} = E_{oc} - NA\ln\left(\dfrac{I_{nom}}{i_0}\right) - R_{ohm}I_{nom} \\ V_{min} = E_{oc} - NA\ln\left(\dfrac{I_{max}}{i_0}\right) - R_{ohm}I_{max} \end{cases} \tag{2-33}$$

This gives:

$$\begin{cases} NA = \dfrac{(V_1 - V_{nom})(I_{max} - 1) - (V_1 - V_{min})(I_{nom} - 1)}{\ln(I_{nom})(I_{max} - 1) - \ln(I_{max})(I_{nom} - 1)} \\ R_{ohm} = \dfrac{V_1 - V_{nom} - NA\ln(I_{nom})}{I_{nom} - 1} \\ i_0 = e^{\left(\frac{V_1 - E_{oc} + R_{ohm}}{NA}\right)} \end{cases} \tag{2-34}$$

2.4.2.3 Model output

The output of the model are the stack voltage (V) and power (kW)

2.4.3 The Detailed model

The detailed model represents a particular fuel cell stack when the parameters such as pressures, temperature, compositions and flow rates of fuel and air vary. These variations affect the Tafel slope (A), the exchange current (i_0) and the open circuit voltage (E_{oc}).

The equivalent circuit of the detailed model (shown in figure 7) is the same as for the simplified one, except that the parameters (E_{oc}, i_o, A) will have to be updated based on the input pressures and flow rates, stack temperature and gases compositions.

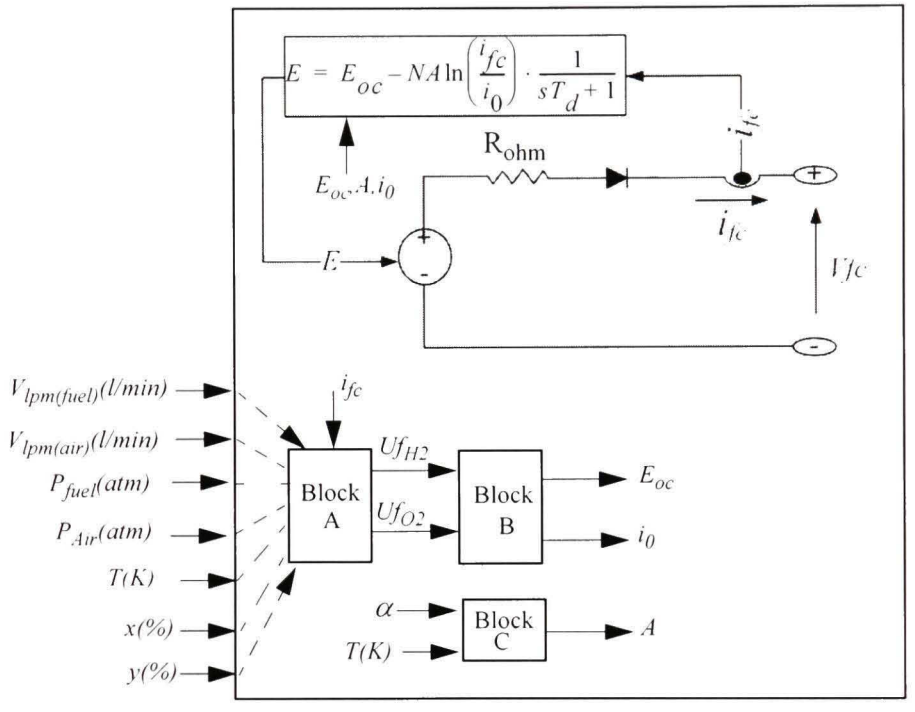

Figure 7 ***Equivalent circuit for the detailed model.***

The open circuit voltage is proportional to the Nernst voltage. At no current, the hydrogen and oxygen utilization are null and the Nernst voltage depends only on the inlet pressures. When the current is greater than zero, the Nernst voltage depends on both the utilizations and inlet pressures. The open circuit voltage is then given by:

$$E_{oc} = \begin{cases} K_i E_n & i_{fc} \le 0 \\ K_c E_n & i_{fc} > 0 \end{cases} \qquad (2\text{-}35)$$

Where K_i and K_c are constants.

In figure 7, firstly, Block A calculates the utilizations using equations (2-16). Then, Block B calculates the open circuit voltage and the exchange current using equations (2-35) and (2-25). Finally Block C calculates the Tafel slope using (2-22). These blocks are added easily to the SPS simplified model.

When the input flow rates are zero or the maximum current is reached, the Nernst voltage is reduced exponentially to limit the output power. The full view of the model is shown in appendix A.

2.4.3.1 Data required for parameters determination

For the detailed model, in addition to (E_{oc}, R_{ohm}, i_o, NA), five more parameters (α, ΔG, K, K_i, K_c) are to be determined. Therefore, in addition to the four points on the polarization curve and the stack response time, the following variables are needed:

a. Number of cells in series (N)
b. Nominal LHV stack efficiency (η_{nom}) in %
c. Nominal operating temperature (T_{nom}) in ^{o}C
d. Nominal air flow rate ($V_{air(nom)}$) in liter/min
e. Absolute supply pressures ($P_{fuel(nom)}$, $P_{air(nom)}$) in atm
f. Nominal composition of fuel and air (x_{nom}, y_{nom}, w_{nom}) in %
g. Voltage undershoot (V_u) in V

A guide showing the procedure to extract these data from stack's datasheet is attached in appendix B.

2.4.3.2 Parameters determination

The parameters (E_{oc}, R_{ohm}, i_o, NA) are determined exactly as in the simplified model. The remaining parameters are determined using the set of equations shown in Table IV

Table IV

Parameters determination for the detailed model

Parameters	Equations
α	$\alpha = \frac{NRT_{nom}}{zFNA}$
ΔG	$\Delta G = -RT_{nom} \cdot \ln\left(\frac{i_0}{K_1}\right)$ $K_1 = \frac{2Fk(P_{H_2(nom)} + P_{O_2(nom)})}{hR}$ $P_{H_2(nom)} = x_{nom}\%(1 - U_{f_{H_2}(nom)})P_{fuel(nom)}$ $P_{O_2(nom)} = y_{nom}\%(1 - U_{f_{O_2}(nom)})P_{air(nom)}$ $U_{f_{H_2(nom)}} = \frac{\eta_{nom}\Delta h°(H_2O(gas))N}{2FV_{nom}}$ $U_{f_{O_2(nom)}} = \frac{60000RT_{nom}NI_{nom}}{2zFP_{air(nom)}V_{air(nom)}y_{nom}\%}$
K_i and K_c	$K_i = \frac{E_{oc}}{E_{n_0}}, E_{n_0} = E_n\big\vert_{U_{f_{H_2}} = 0,\ U_{f_{O_2}} = 0}$ $K_c = \frac{E_{oc}}{E_{n_{(nom)}}}$ $E_{n_{(nom)}} = E_n\big\vert_{U_{f_{H_2}} = U_{f_{H_2(nom)}},\ U_{f_{O_2}} = U_{f_{O_2(nom)}}}$
K	$K = \frac{V_u}{K_c(U_{f_{O_2}(max)} - U_{f_{O_2}(nom)})}$ $U_{f_{O_2}(max)} = 0.6$

A maximum oxygen utilization during transient is assumed to be equal to 60 % as most fuel cells operate with output inductors which limit the rate of increase of current. Normally, fuel cells operate with oxygen utilization around 50%.

The Matlab-file used to calculate the parameters is attached in appendix C.

2.4.3.3 Model inputs

The inputs to the model are the following:

a. Operating temperature (^{o}K)
b. Supply pressures of gases (atm or bar)
c. Gas flow rates at inlet (liter/minute)
d. Gas compositions (%H_2 in the fuel, %O_2 and %H_2O in air)

2.4.3.4 Model outputs

The model outputs are:

a. Stack voltage (V) and power (kW)
b. Fuel and air consumptions in standard liter per minute (slpm)
c. Stack efficiency (%)

2.5 Model limitations

The following are the limitations of the model:

a. Chemical reaction dynamics caused by the variation of partial pressure of species inside the cell is not considered
b. The flow of gases or water through the membrane is not taken into account

c. The effect of temperature and humidity of the membrane on the stack resistance is not considered

d. The stack output power is limited by the fuel and air flow rates supplied

2.6 Conclusion

In this chapter, a fuel cell stack model is developed and implemented in SPS. The modeling equations which make up the model are derived and the model assumptions are stated.

Two models are proposed along with their equivalent circuits. The parameters required in the model are determined based on data provided by the user. These data are obtained easily from fuel cell manufacturer's datasheet. The model inputs/outputs variables are mentioned and its limitations are stated.

The main advantage of these models compared to the previous model developed in the literature is that no test is required on real fuel cells or data treatment and calculations prior to simulation. In addition, these models are generic models and able to emulate the behavior of any fuel cells types fed with hydrogen and air.

The next chapter discusses the validation of these models and presents a correlation between the model behavior and the real stack's performance.

CHAPTER 3

MODEL VALIDATION

3.1 Introduction

This chapter focuses on the validation of the proposed models. A 6kW-45V PEMFC stack is modeled and its steady state performance is validated by comparing the polarization curve obtained in simulation with the real curve from the datasheet.

Data provided by most stack manufacturers are usually at nominal condition of operation and do not give a clear insight as to how the stack performance changes with parameters such as gases pressure, flow rates and temperatures.

In order to observe the effect of these parameters, experiments are performed on the EPAC-500 (500W-48V, PEMFC stack) at different conditions of operation. A detailed model of the stack is made and the simulation results are compared with the test results to ascertain the validity of the model.

3.2 Model validation in steady state, nominal condition

A model of a 6kW-45V, PEMFC stack (the NedStack PS6) from NedStack is made using its datasheet. Data are extracted as described in appendix B and the model parameters are determined.

The simplified model and the detailed model are equivalent at nominal condition of operation (as their model parameters are equal).

The polarization curves obtained in steady state from both models are superimposed on the datasheet curve as shown in figure 8.

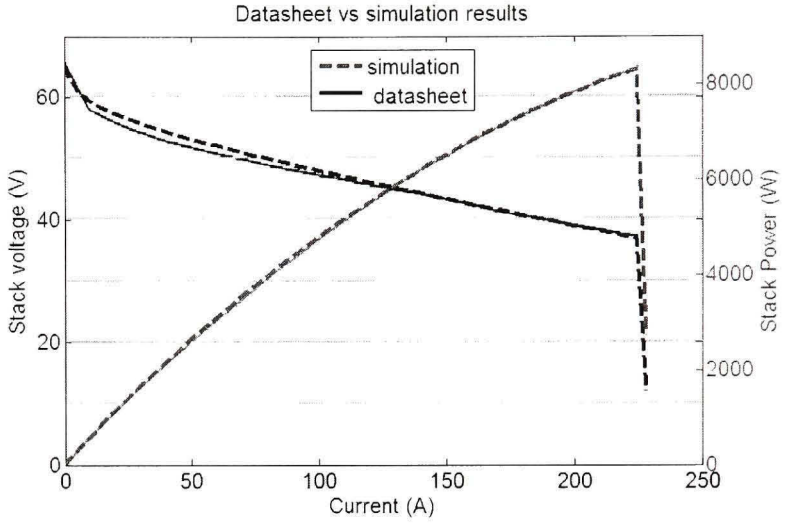

Figure 8 ***Simulation and datasheet results.***

The dotted line shows the simulated curve whereas the solid line is the real curve from datasheet. It is observed that the simulated curve matches exactly the real one in the ohmic region. A difference is observed in the activation region due to the non-linearity of the activation voltage (more points are needed at low current to determine a better value of i_0 and α).

The same result will be obtained for any type of fuel cells as they all have similar polarization curves.

Considering that most fuel cells operate in the ohmic region, the proposed models are therefore adequate for steady state simulation of fuel cells power systems. The level of accuracy of the model depends on the precision of data provided by the user.

3.3 Model validation at different conditions of operation

A 500W-48V fuel cell stack (EPAC-500) from Hpower is used to observe the stack behavior when gas pressures, flow rates and temperature change. The stack and the test setup are provided by Institut de recherche sur l'hydrogène (IRH) in Trois-Rivières.

The test setup (shown in figure 40, appendix D) allowed the variation of the following parameters:

a. *Inlet pressures of gases:* Hydrogen is kept in a high pressure tank and its inlet pressure is set manually using a pressure valve. A compressor is used to pressurize the inlet air. Air inlet pressure is set by the user from the LabVIEW mask (shown in figure 41, appendix D). Both inlet pressures can be varied from 15 kPa to 35 kPa (relative pressure).

b. *Inlet flow rates of gases:* Flow rate regulators are used to allow the variation of inlet flow rates. As there is no return path for the hydrogen from the stack outlet to the tank, it is not possible to operate the stack at fixed hydrogen flow rate (hydrogen will be wasted). Therefore the stack always operates at hydrogen utilization closed to 100%. For air, it is possible to impose any flow rate (starting from 10 slpm) or to operate at any oxygen utilization (maximum of 50%). Air flow rate and oxygen utilization references are given through the LabVIEW mask.

c. *Stack temperature:* Air cooling is used to control the stack temperature. There are temperature sensors throughout the stack and the average temperature is controlled by varying the input voltage of fans. The temperature can be varied from 27 °C to 50 °C.

d. *Load current or power:* An electronic load is used and the user can vary the fuel cell current or power via the LabView mask.

In order to compare the test and the simulation results when these parameters change, a detailed model is necessary.

3.3.1 The stack model

As the stack's datasheet is not available, a performance test at a given condition of operation is required to obtain data such as the polarization curve, efficiency, stack response time etc., which will be used to determine the parameters of the model.

Figure 9 shows the test results at hydrogen and air inlet pressures of 35 kPa and 25 kPa respectively.

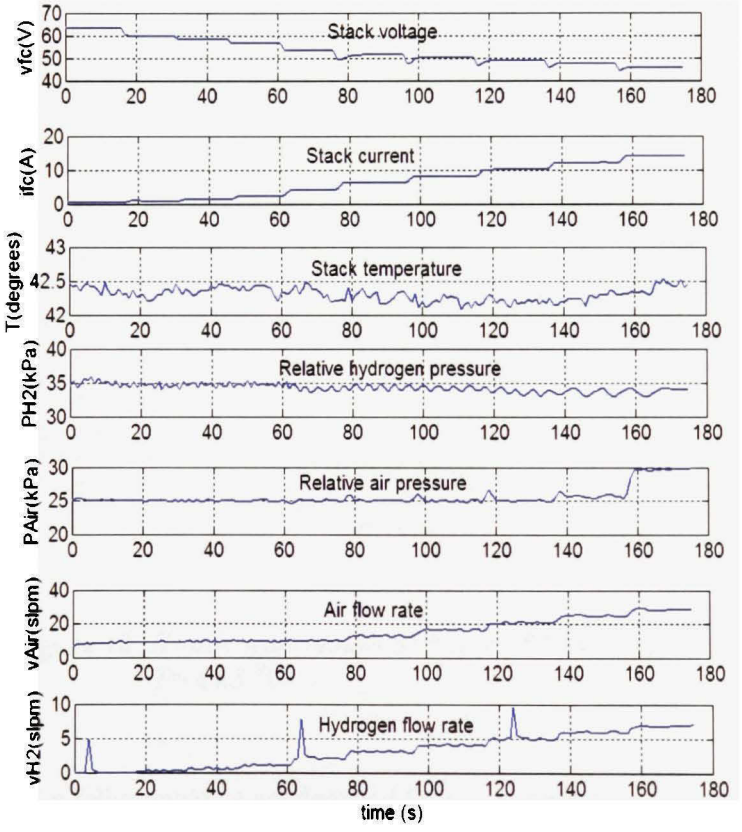

Figure 9 ***Test results at P_{Air} = 25 kPa, P_{H2} = 35 kPa, T= 42.3 ^{o}C.***

From figure 9, the polarization curve is obtained by taking ten points on the vfc-time characteristic. These points are chosen in steady state and at similar gas utilizations. Figure 10 shows the derived polarization curve along with the stack temperature, gas pressures and utilizations. It can be noted that the hydrogen utilization gets higher than 100% at low current. This is due to the fact that at lower current, the residue of hydrogen inside the stack contributes in the reaction.

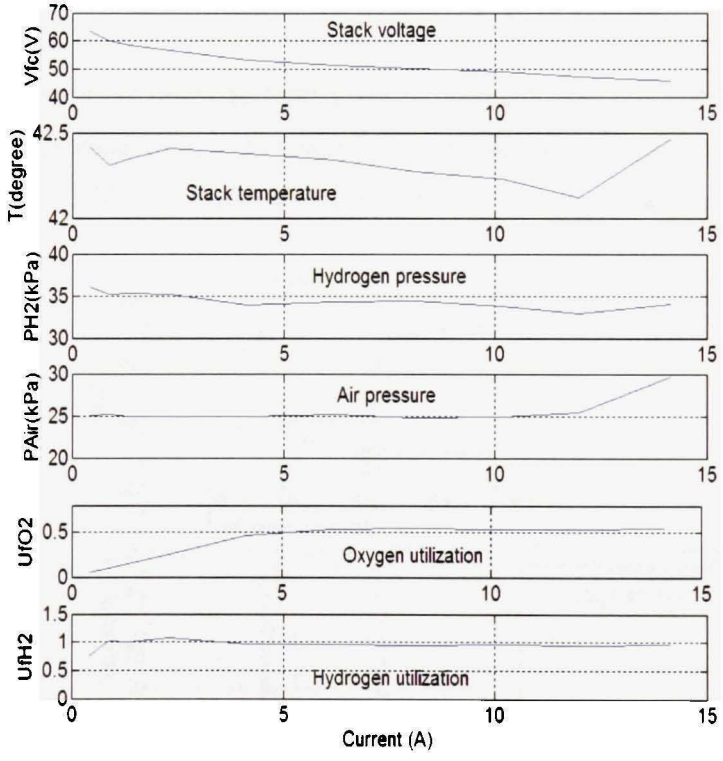

Figure 10 ***Steady state results at P_{Air} = 25 kPa, P_{H2} = 35 kPa, T= 42.3 °C.***

From figure 10, the following data are deduced for model parameters determination:

a. $(I_{nom}, V_{nom}) = (8.128, 50.28)$

b. $(I_{max}, V_{min}) = (14.155, 45.707)$

c. $(E_{oc}, V_l) = (65.7, 58.4)$

a. $N = 65$ (this value is mentioned on the stack)

b. $\eta_{nom} = 58.83\%$ (using equation (2-29))

c. $T_{nom} = 42.3^{o}C$

d. $V_{air(nom)} = 14.91$ liter/min (using equation (2-16))

e. $(P_{fuel(nom)}, P_{air(nom)}) = (1.35, 1.25)$

Figure 11 shows the result obtained from a current interrupt test. From this test, parameters such as the stack response time, compressor delay, voltage undershoot can be estimated. We have $T_d = 1$s, $V_u = 2.5$ V and compressor delay = 1s.

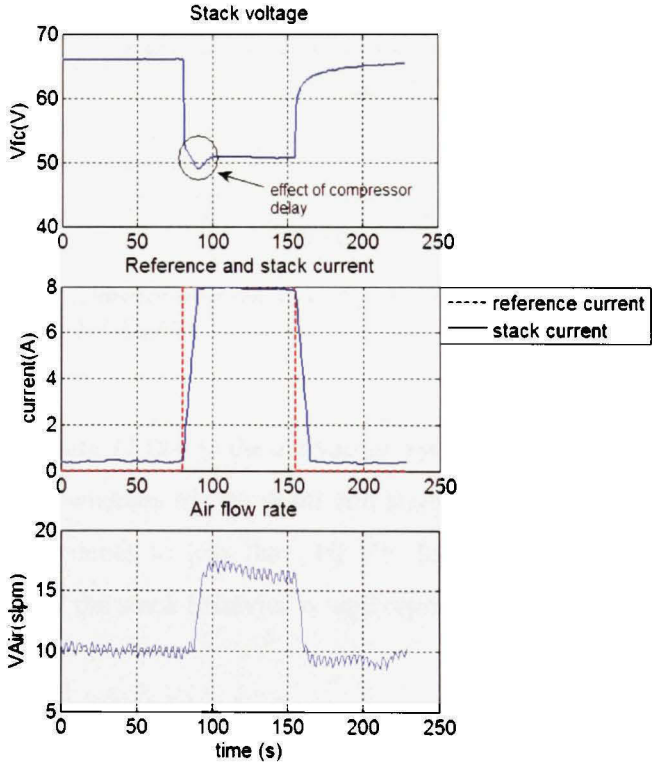

Figure 11 ***Current interrupt test.***

The parameters of the model are determined and the stack is simulated at the same condition of temperature, gas pressures and utilizations.

Figure 12 shows the simulation results along with the percentage error between the simulated and the real output voltage.

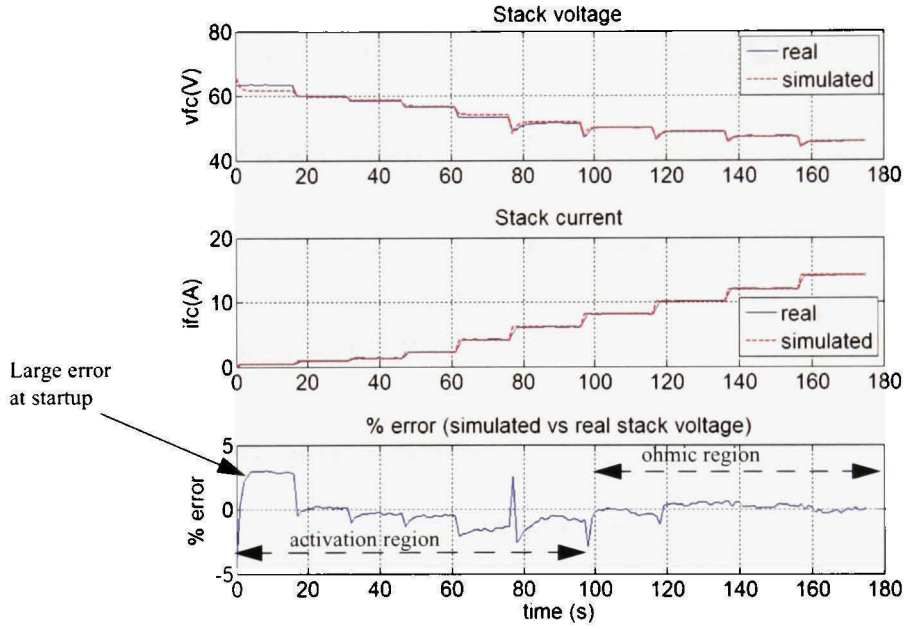

Figure 12 ***Simulation results at P_{Air} = 25 kPa, P_{H2} = 35 kPa, T= 42.3 °C.***

It can be observed from figure 12 that in the activation region, the steady state error is within $\pm 1\%$ at normal operation whereas the transient and startup errors are within $\pm 3\%$. In the ohmic region, the error reduces to less than $\pm 0.5\%$ for both transient and steady state conditions. This shows that the stack behavior is well represented by the model.

The large error at startup is mainly due to the residues of hydrogen and oxygen inside the stack at the beginning of the experiment. This makes the real reactant utilizations much greater than the simulated utilizations.

Now having the stack model, it is possible to submit both the stack and the model to different conditions of operation and compare their behavior. The following variations on the condition of operation are made:

a. Variation of inlet pressures of gases at constant stack temperature
b. Variation of stack temperature at constant inlet pressures
c. Variation of inlet air flow rate at constant stack temperature and inlet pressures

3.3.2 Variation of inlet pressures of gases at constant stack temperature

Figures 42, 43, and 44 in appendix D show the test results at (P_{Air} , P_{H2}) = (15 kPa, 15 kPa), (P_{Air} , P_{H2}) = (25 kPa, 23.5 kPa) and (P_{Air} , P_{H2}) = (35 kPa, 33 kPa) respectively. The stack temperature is held constant to 42 °C.

The simulation and test results at same conditions are shown in figures 13, 14 and 15.

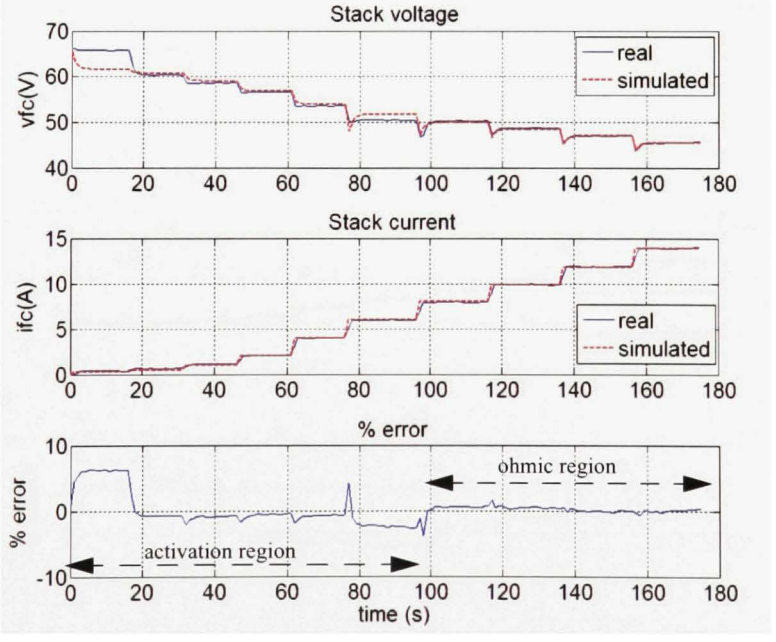

Figure 13 ***(P_{Air}, P_{H2}) = (15 kPa, 15 kPa), T= 42°C.***

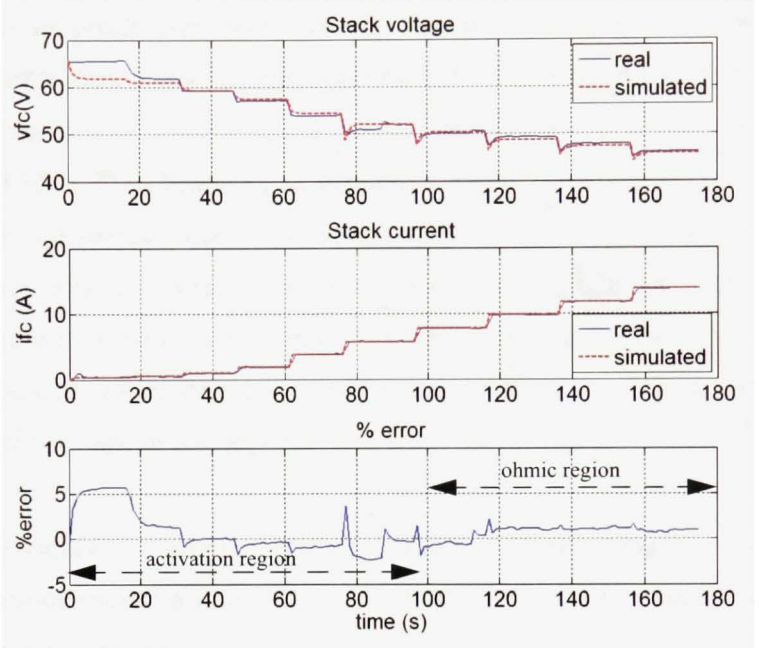

Figure 14 $(P_{Air}, P_{H2}) = (25\ kPa, 23.5\ kPa)$, $T = 42^{o}C$.

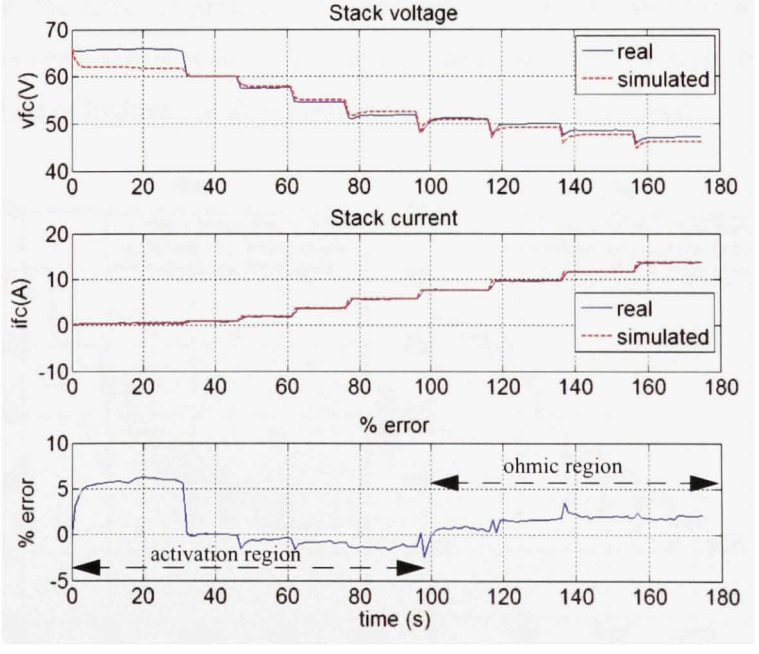

Figure 15 $(P_{Air}, P_{H2}) = (35\ kPa, 33\ kPa)$, $T = 42^{o}C$.

It can be observed from figures 13, 14 and 15 that as the gas pressures increase, the percentage error in steady state does not vary much in the activation region (error less than $\pm 1\%$, except at startup and abnormal operation). In the ohmic region this error increases with pressure (less than $\pm 0.5\%$ at P_{Air} = 15 kPa, closed to 1% at P_{Air} = 25 kPa and closed to 2% at P_{Air} = 35 kPa). This difference in the ohmic region is mainly due to the fact that the stack resistance is assumed to be constant in the model at all conditions of operation. In reality, as the air pressure increases, the relative humidity inside the stack increases, this means cell's membrane gets more humid. This increases the membrane conductivity and therefore the stack resistance decreases. This explains why the real stack voltage is greater than the simulated voltage in that region.

For P_{Air} = 15 kPa and P_{Air} = 25 kPa, the humidity inside the cell is lower or close to its value at nominal condition (nominal humidity). This means the resistance doesn't vary much and therefore the error is very low.

Figure 16 shows the effect of pressures on the stack voltage. The increase in stack voltage with pressures is verified experimentally as well as in simulation. The large error at startup is due to the residues of hydrogen and oxygen inside the stack as stated earlier.

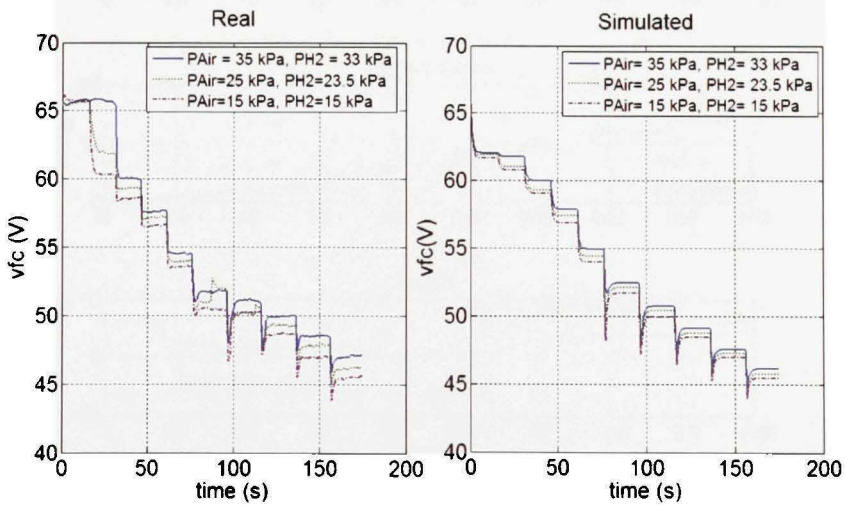

Figure 16 ***Effect of pressure on the stack voltage.***

From the above discussion it can be stated that the effect of pressure on the stack performance is well represented by the model (the model and the real stack have similar behavior as the pressure changes). If the stack is equipped with a water management system (as most PEMFC fuel cell systems do) to maintain the level of humidity constant, then the error between the simulated voltage and the real voltage will be within $\pm 1\%$, this is true in steady state as well as in transient state. However, the model gives an error of 1% for every 9% increase in air pressure due to the effect of humidity.

3.3.3 Variation of stack temperature at constant inlet pressures

Figures 45, 46 and 47 in appendix D show the tests results at T= 35 °C, T= 39 °C and T= 46°C respectively. Both air and hydrogen inlet pressures are maintained at 35 kPa.

Figures 17, 18 and 19 show the stack voltage (simulated and real) along with the percentage error obtained at each stack temperature respectively.

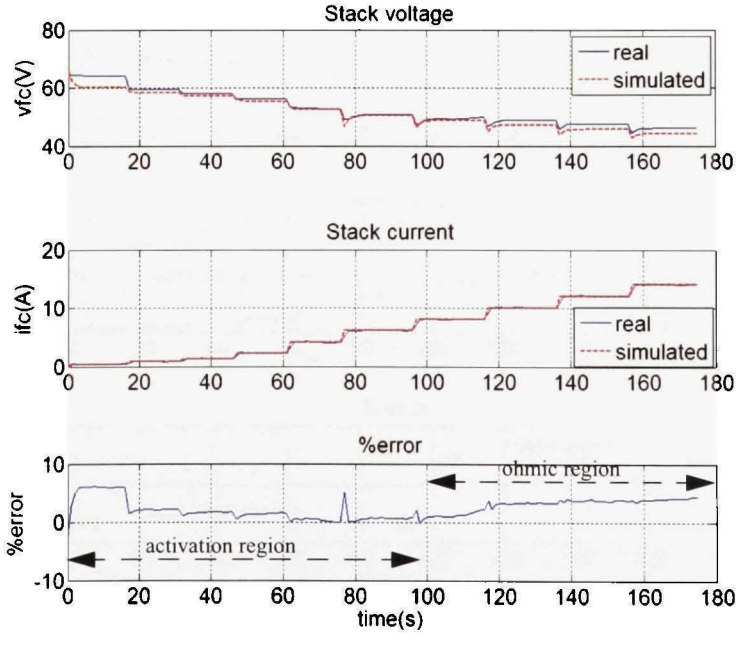

Figure 17 $(P_{Air}, P_{H2}) = (35\ kPa, 35\ kPa)$, $T = 35\ ^{o}C$.

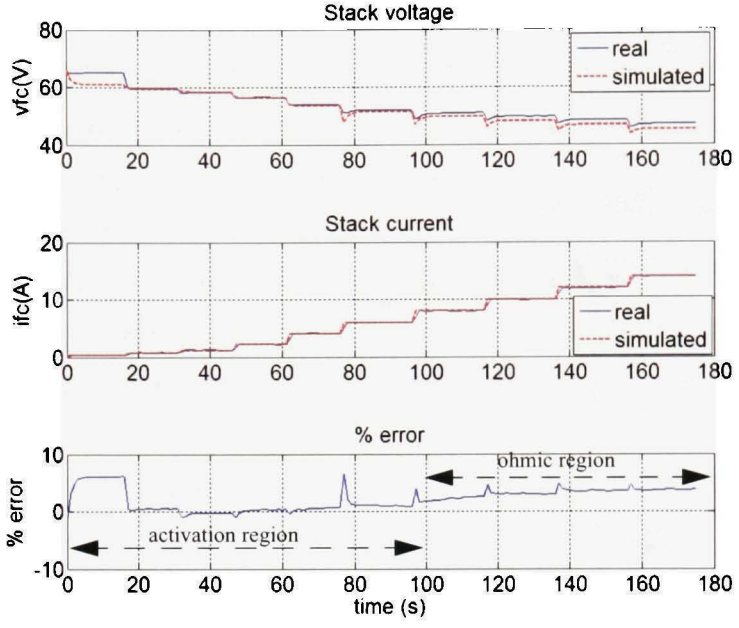

Figure 18 $(P_{Air}, P_{H2}) = (35\ kPa, 35\ kPa), T = 39^{o}C$.

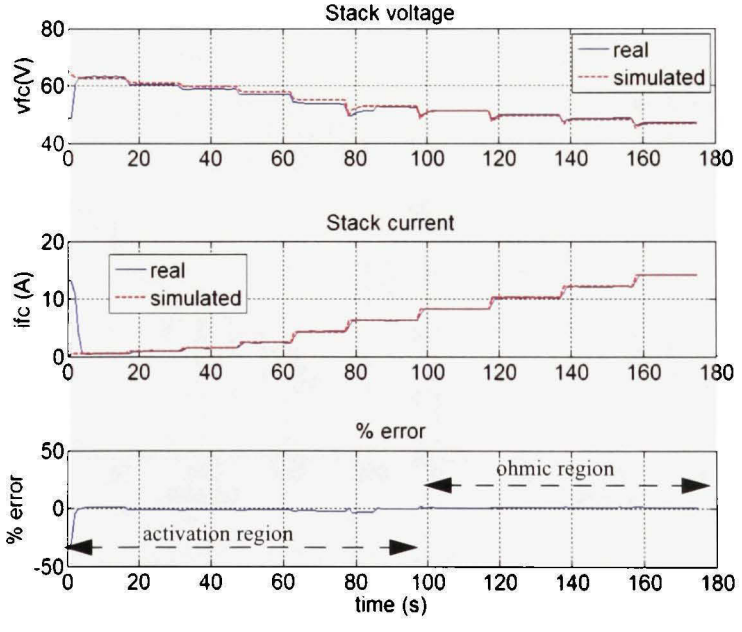

Figure 19 $(P_{Air}, P_{H2}) = (35\ kPa, 35\ kPa), T = 46^{o}C$.

It can be observed from figures 17, 18 and 19 that as the stack temperature increases, the percentage error in steady state reduces in the activation region (% error closed to 2% at 35 °C, closed to 1% at 39 °C and within ±0.5% at 46 °C). In the ohmic region, at 35 °C and 39 °C, this error is around 4% and at 46 °C, it reduces to less than 1%. This difference in the activation and ohmic regions can be explained from the fact that at lower stack temperature, the relative humidity inside the stack is higher, and therefore the cell's membrane is more humid. This increases the membrane conductivity and therefore the stack resistance decreases (that means less resistive losses). As the resistance is assumed to be constant, the real stack voltage will be higher than the simulated voltage.

At 46 °C, the humidity inside the cell is lower or closed to the nominal humidity. The resistance is constant and consequently the error is lower.

Figure 20 shows the effect of temperature on the stack voltage. The increase in stack voltage with temperature is verified experimentally as well as in simulation.

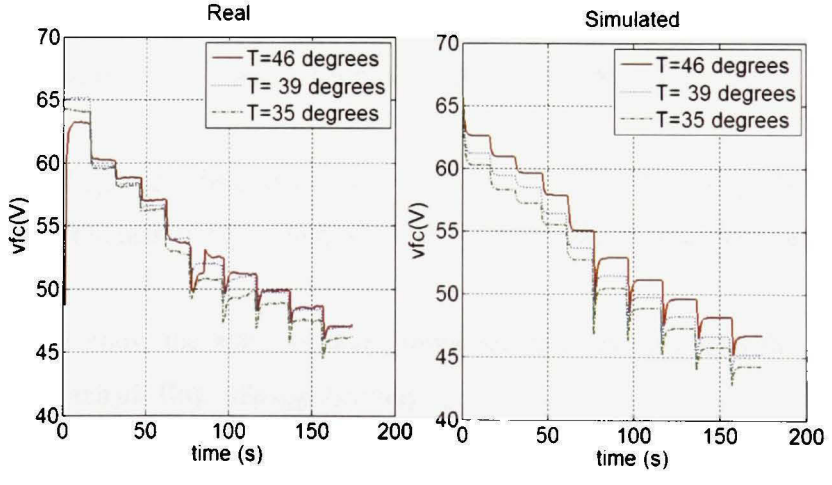

Figure 20 ***Effect of temperature on the stack voltage.***

Normally with the increase in temperature, the stack resistance should decrease (as the mobile ions will move more rapidly). But from figure 20 (real), the resistance does not vary much when the temperature changes from 39°C to 46°C. That is because the effect of membrane humidity counteracts the effect of temperature. This means the membrane conductivity is highly dependent on its water content for PEMFC.

From these results, it can be stated that the effect of temperature on the stack performance is also well represented by the model (the model and the real stack have similar behavior as the temperature changes). If the level of humidity is controlled, then the error between the simulated voltage and the real voltage will be within ±1%. This is valid in steady state as well as in transient state. However, the model gives an error closed 3% for a 15% decrease in temperature due to the effect of humidity.

3.3.4 Variation of inlet air flow rate at constant temperature and pressures

Figures 48 and 49 in appendix D show the tests results at V_{Air} = 25 slpm (23.09 lpm) and V_{Air} = 20 slpm (18.47 lpm) respectively. Air and hydrogen inlet pressures are maintained at 25 kPa and 32 kPa respectively. The stack temperature is constant to 42.3 °C.

In the model, for V_{Air} = 25 slpm, the air inlet pressure is set to 28 kPa for the first 80 s and then to 25 kPa for the last 95 s to match with the experimental inlet air pressure.

Figures 22 and 21 show the stack voltage (simulated and real) along with the percentage error obtained at each air flow rate respectively.

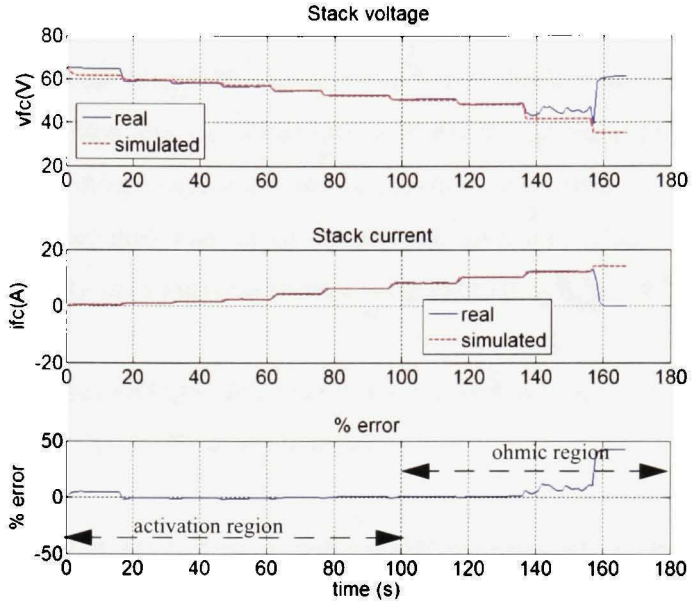

Figure 21 *(P_{Air}, P_{H2}) = (25 kPa, 32 kPa), T= 42.3°C, V_{Air} = 20 slpm.*

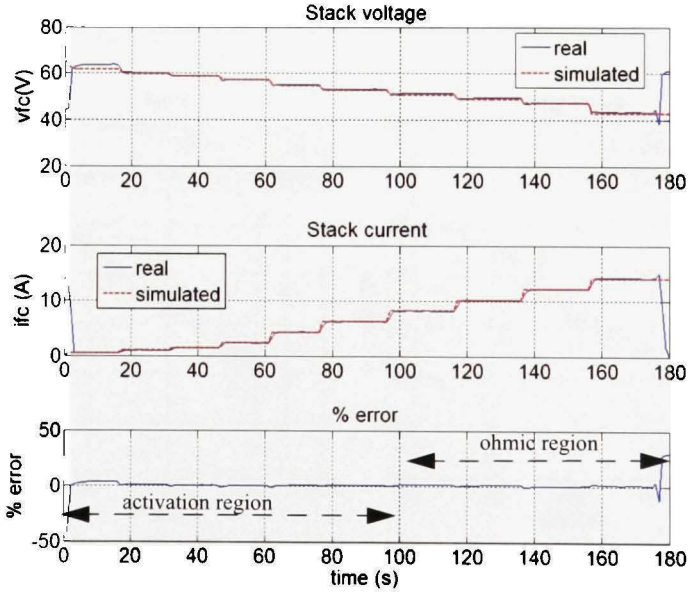

Figure 22 *(P_{Air}, P_{H2}) = (25 kPa, 32 kPa), T= 42.3°C, V_{Air} = 25 slpm.*

It can be observed from figures 22 and 21 that as the air flow rate increases, the percentage error in steady state in both the activation and ohmic region stays within $\pm 0.5\%$ (except at startup and abnormal operation). The lower error in the ohmic region can be explained as follows: with high air flow rate, the water generated doesn't accumulate inside the stack. As we are operating at nominal temperature and air pressure, the humidity inside the stack is the nominal humidity, which means the stack resistance is almost constant in both conditions of operation. Consequently the simulated voltage is closed to the real stack voltage.

It can also be noted that voltage undershoots are not present, this is because there are no delay in the compressor as the flow rate is fixed.

For the safety of the stack, the current is switched-off automatically as one of the cell voltage goes below 0.45 V. This is seen in figures 22 and 21 at 175 s and 155 s respectively.

Figure 23 shows the effect of air flow rate on the stack voltage. The increase in stack voltage with air flow rate is verified experimentally as well as in simulation.

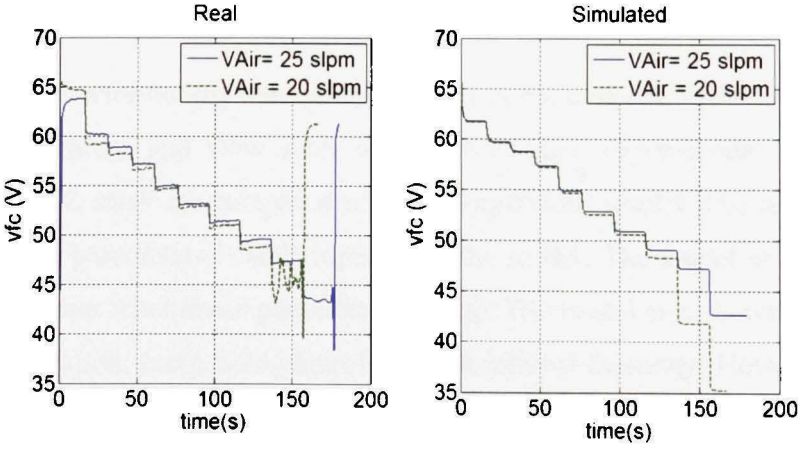

Figure 23 ***Effect of air flow rate on the stack voltage.***

With a lower air flow rate, the stack gets depleted of oxygen at lower current and a fast decrease in output voltage arrives much earlier. From figures 22, 21 and 23, it can be noted that the output voltage starts to decrease rapidly at 135s (when the current is above 10 A) and 165s (when the current is above 14 A) for V_{Air} = 20 slpm and V_{Air} = 25 slpm respectively.

From these results, it can be stated that the effect of flow rate on the stack performance is well represented by the model (the model and the real stack have similar behavior as the air flow rate changes). The error between the simulated voltage and the real voltage is very low (within $\pm 0.5\%$). This result is valid in steady and transient states.

3.4 Conclusion

In this chapter, the validation of the simplified and detailed model is made. Both models are validated in steady state and at nominal condition of operation using data from a stack datasheet. The steady state simulation of a 6kW-45V PEMFC stack from NedStack gives a V-I curve very close to the one given by the manufacturer. This result is valid for any type of fuel cells.

To validate the behavior (steady state and transient) of the detailed model when parameters (pressures, temperature and flow rates of gases) change, experimental results from a 500W-48V PEMFC stack are compared with the simulations results. The results show that the effect of these parameters is well captured in the model. The model and the real stack have similar behavior when these parameters change. The model error is within $\pm 1\%$ at all conditions of operation, provided a controlled stack internal humidity. However, the model gives an error of 1% for every 9% increase in air pressure and an error of 3% for a 15% decrease in temperature due to the effect of humidity.

The proposed models being valid, these models are integrated in SPS and the model's performance is observed in a simulation of a fuel cell electric vehicle (FCV). The next chapter presents the integrated model in SPS and a demonstration (demo) of the FCV.

CHAPTER 4

MODEL APPLICATION: A FUEL CELL VEHICLE

4.1 Introduction

This chapter presents briefly the fuel cell stack model integrated in SPS and its performance in a fuel cell vehicle. The model is integrated in SPS by Olivier Tremblay and is used in a fuel cell vehicle demonstration. The FCV is a typical application of fuel cells and the demo is presented in this report to point out the advantages of the proposed model in the simulations of fuel cell power systems and to show how it inter-acts with other electrical systems.

The demo was developed by myself, Njoya Motapon Souleman and Olivier Tremblay based on the characteristics of the new vehicle developed by Honda (the FCX clarity-2008). I designed the fuel cell stack and the energy management of the powertrain and Olivier took care of the rest of the systems (Battery, AC permanent magnet motor, vehicle dynamics and system integration).

This chapter is subdivided into 3 parts: the first part concerns the presentation of the fuel cell stack model integrated. The second part discusses briefly the FCV demo subsystems. Finally the last part focuses on the simulation results and the performance of the stack in the FCV. The FCV model and the stack performance are validated by comparing the simulation results to the real results obtained from the FCX clarity.

4.2 The SPS fuel cell stack model

The simplified and detailed models implemented in SPS (from chapter 2) are modified to conform to SPS models norms, so to facilitate their integrations in SPS. Figure 24 shows the model icon and the dialog box in which the user enters data extracted from datasheet.

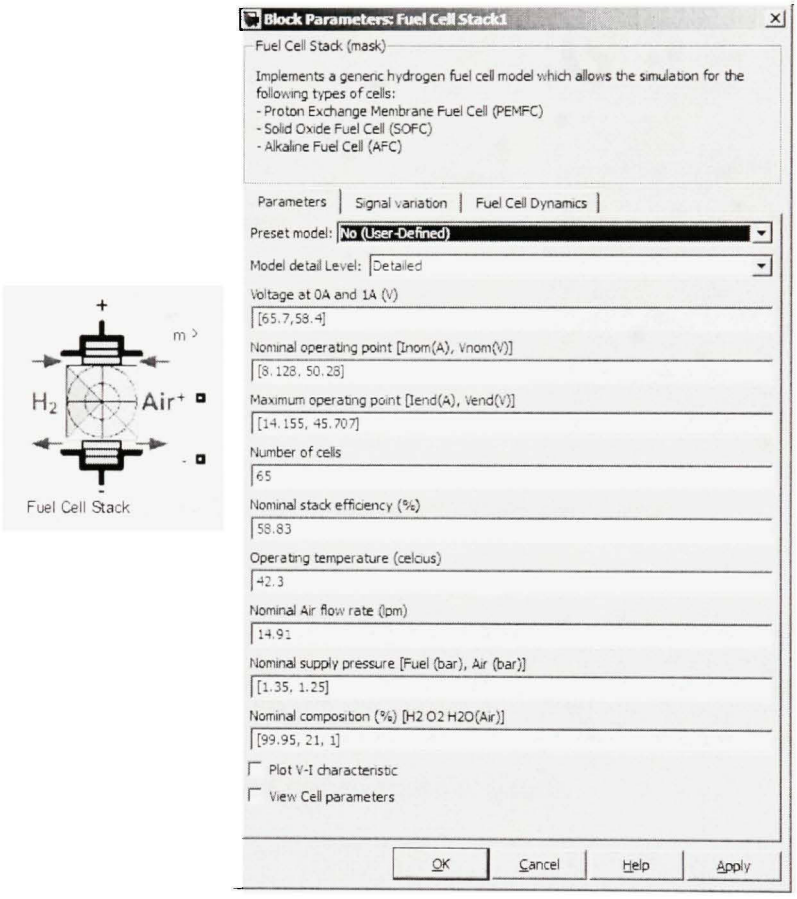

Figure 24 ***Model icon and dialog box.***

The user is able to choose whether to use the simplified or the detailed model from *model detail level* parameter on the dialog box. It is also possible to view the corresponding polarization curve and the stack parameters by checking the *Plot V-I characteristic* and *View cell parameters* boxes.

The dialog box shown in figure 24 contains information of the EPAC-500 discussed in the previous chapter. The corresponding polarization curve and stack parameters are shown in figure 25.

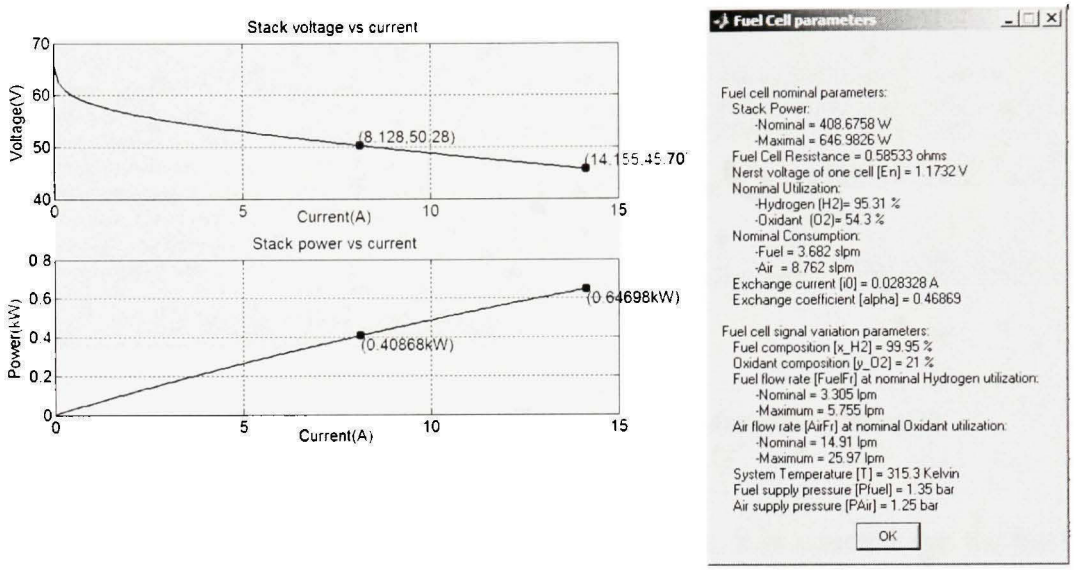

Figure 25 ***Polarization curve and stack parameters.***

The stack parameters dialog box shows the values of parameters such as the stack resistance (R_{ohm}), the Nernst voltage of a cell (E_n), the exchange current (i_0) and the exchange coefficient (α). It provides also information on the nominal condition of operation (temperature, pressures, flow rates and compositions of gases).

This condition of operation can be varied through the *Signal variation* pane. The cell dynamics can also be specified through the *Fuel cell dynamics* pane. These panes are shown in figure 26.

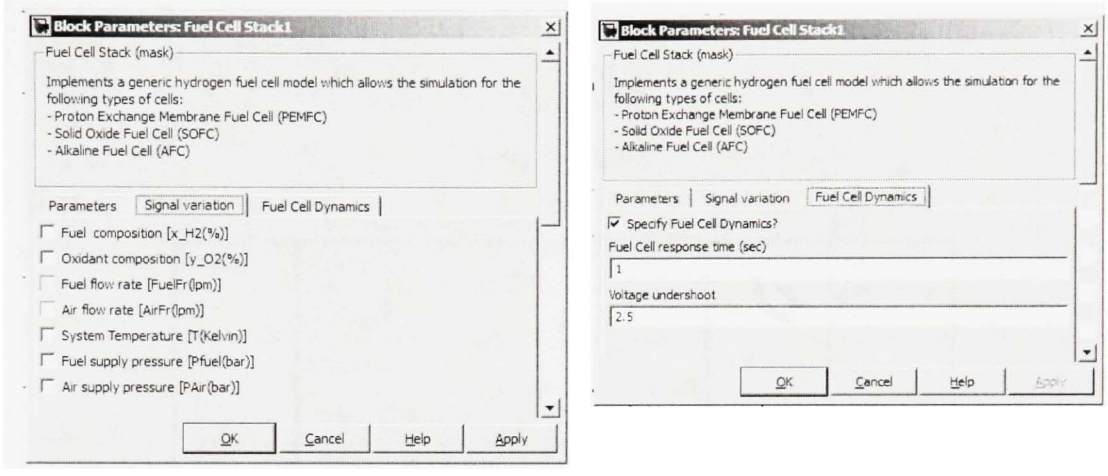

Figure 26 ***Parameters variations and cell dynamics panes***.

In case the user does not provide the fuel and air flow rate, it is assumed that the stack is operating at fixed utilization of gases (nominal utilizations) and the supply of gases is adjusted according to the load current.

The user can use the *preset model* parameter on the dialog box to load the parameters of some predefined fuel cell stack (some PEMFC and AFC stacks available in the market are preset in the model).

The maximum current the stack can deliver is limited by the maximum flow rates of fuel and air which can be reached.

The model outputs 11 signals shown in table V along with their definitions, units and symbols.

Table V

Model outputs

Signal	Definition	Units	Symbol
1	Voltage	V	V_{fc}
2	Current	A	I_{fc}
3	Stack Efficiency	%	η
4	Stack consumption [Air, Fuel]	slpm	V_{slpm}
5	Flow Rate [Air, Fuel]	lpm	Fr_{lpm}
6	Stack consumption [Air, Fuel]	lpm	V_{lpm}
7	Utilization [Oxygen, Hydrogen]	%	U_f
8	Slope of the Tafel curve	V	A
9	Exchange current	A	i_0
10	Nernst voltage	V	E_n
11	Open circuit voltage	V	E_{oc}

4.3 The FCV demonstration

The full diagram of the FCV demo is shown in figure 27. It consists of 3 subsystems which are: the electrical subsystem, the energy management subsystem and the vehicle dynamics subsystem. The later subsystem concerns the modeling of all the mechanical part of the vehicle and is not covered in this report.

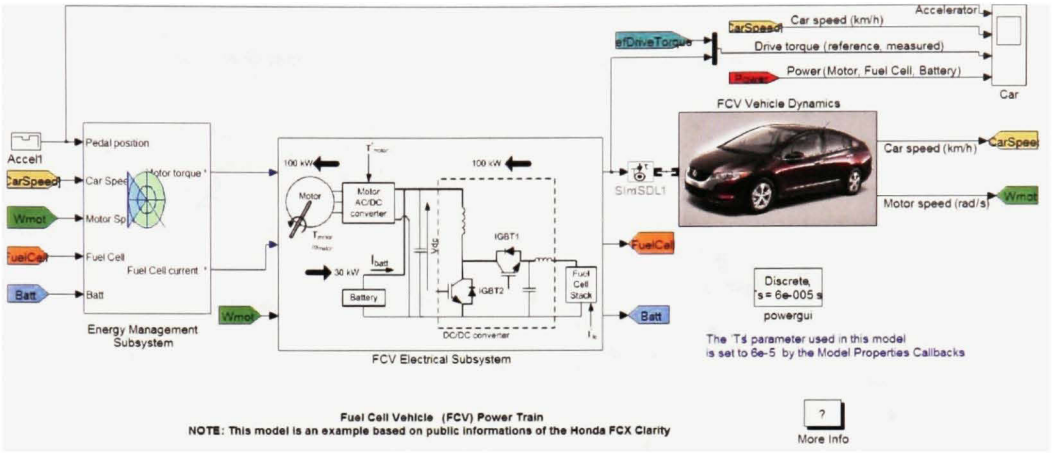

Figure 27 ***The FCV subsystems in SPS.***

4.3.1 The electrical subsystem

The FCV Electrical Subsystem consists of the following parts:

a. The electrical motor: is a 288 Vdc, 100 kW interior Permanent Magnet Synchronous Machine (PMSM) with the associated drive. This motor has 8 pole and the magnets are buried (salient rotor's type). A flux weakening vector control is used to achieve a maximum motor speed of 12 500 rpm. The motor current is controlled from the reference torque deduced from the drive power.

b. The battery: is a 13.9 Ah, 288 Vdc, 25 kW Lithium-Ion battery.

c. The fuel cell stack: is a 400 cells, 288 Vdc, 100 kW Proton Exchange Membrane (PEM) fuel cell stack.

d. The DC/DC converter: is an average value buck converter with a current regulator.

The full diagram of this subsystem is shown in figure 28

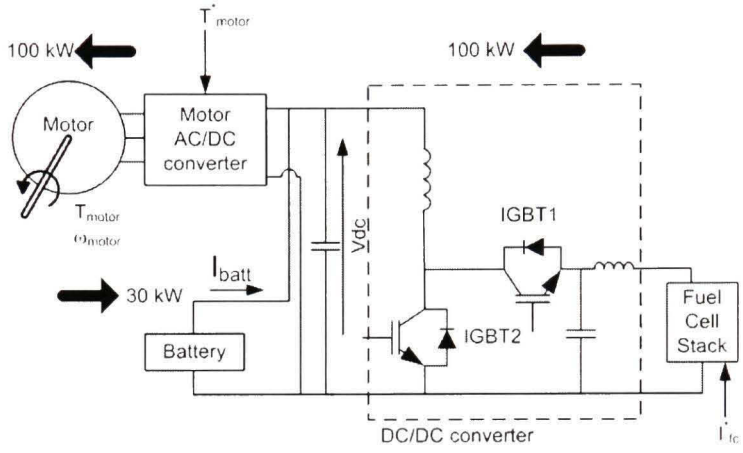

Figure 28 ***The FCV powertrain.***

The elements of concern in this report are the fuel cell stack and its connection to the system. Therefore the model of the stack and the DC-DC converter will be briefly described in the following lines.

4.3.1.1 The fuel cell stack

A detailed model of the fuel cell stack is selected for the simulation. The only information given by Honda (Honda FCX Clarity Press Kit, 2008) is the stack nominal voltage and power (288V-100kW) and the condition of operation (3bar, 95°C).The others parameters are estimated as follows:

a. Maximum point of operation = [347.3 A, 288 V]
b. Nominal point of operation (85% of 100 kW) = [285 A, 300 V]
c. Number of cell in series = 400 (288V / 0.7 V)
d. Stack temperature = 95 °C
e. Stack efficiency: $\eta = \frac{zF \times 300 \times 0.95}{\Delta h^{\circ}(H_2O(gas)) \times 400} \times 100 \approx 57\%$
f. Air and H_2 pressure = 3 bar

g. H_2 and Air are assumed to 99.95% H_2 et 21% O_2 respectively

h. The stack response time is assumed to be 2 s

i. Nominal air flow rate: $V_{air(nom)} = \frac{60000 RT_{nom} NI_{nom}}{2zFP_{air(nom)} \times 0.21 \times 0.5} \approx 1698 \ lpm$

Figure 29 shows the stack information along with its parameters.

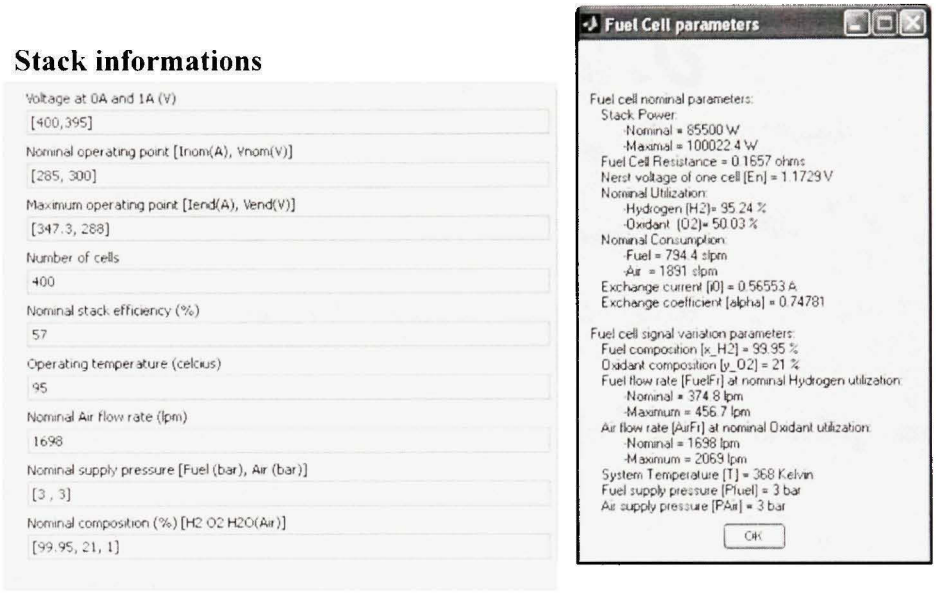

Figure 29 ***The Fuel cell stack information.***

The stack inlet flow rate depends on the reference current as shown in figure 30. The flow rates are calculated using equation (2-16). This reference current depends on the fuel cell power demanded, which is proportional to the drive power.

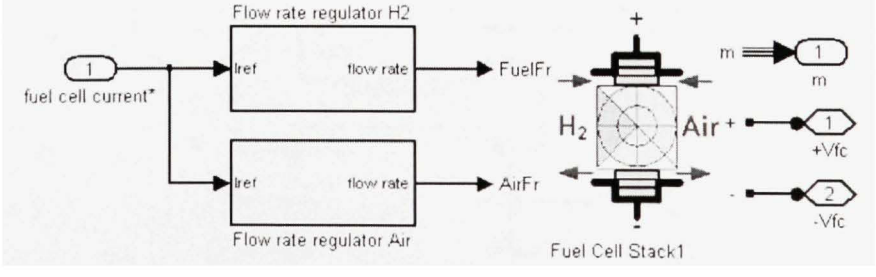

Figure 30 ***Stack with flow rate regulators.***

The stack polarization curve is shown in figure 31. The stack voltage varies from 400V to 288V.

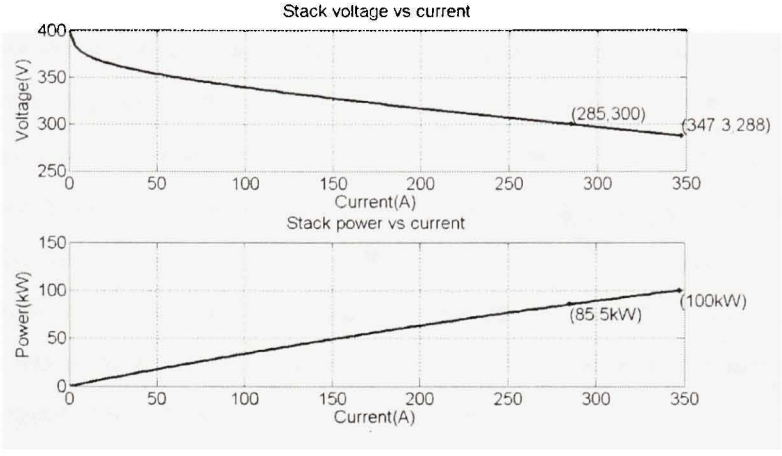

Figure 31 ***Stack polarization curve.***

As the DC bus or battery voltage is 288V, the use of a step down DC-DC converter is necessary to connect the stack to the DC bus.

4.3.1.2 The DC-DC converter

An average value model of the DC-DC buck converter is used here to allow a fast simulation of the systems. The converter circuit is shown in figure 28. A filter is connected at the stack output to reduce the rate of change of the fuel cell current. A simple PI controller is used to control the fuel cell current. The controller reference current is the same as the fuel cell stack current reference. This is shown in figure 32.

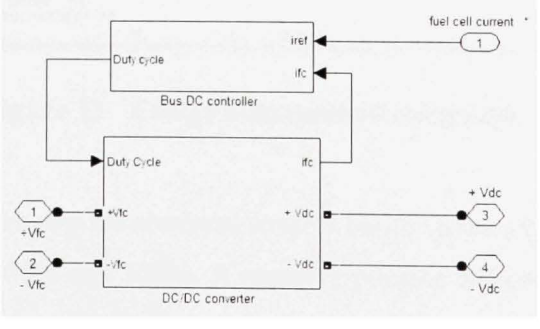

Figure 32 ***DC-DC converter (Simulink).***

4.3.2 The energy management subsystem

In order to accurately distribute the power between the battery and the fuel cell stack, an energy management strategy is necessary. The energy management subsystem determines the motor torque and the fuel cell current references based on the pedal (accelerator) position, the car speed, the motor speed and the fuel cell voltage. It consists of 3 blocks: the first block calculates the drive power (using the characteristic Torque-car speed provided by Honda) and the last 2 blocks calculate the reference torque and fuel cell current. The polarization curve at nominal condition of operation is used to determine the fuel cell current reference. The torque reference depends on the demanded total power (battery + fuel cell) and the motor speed. These blocks are shown in figure 33.

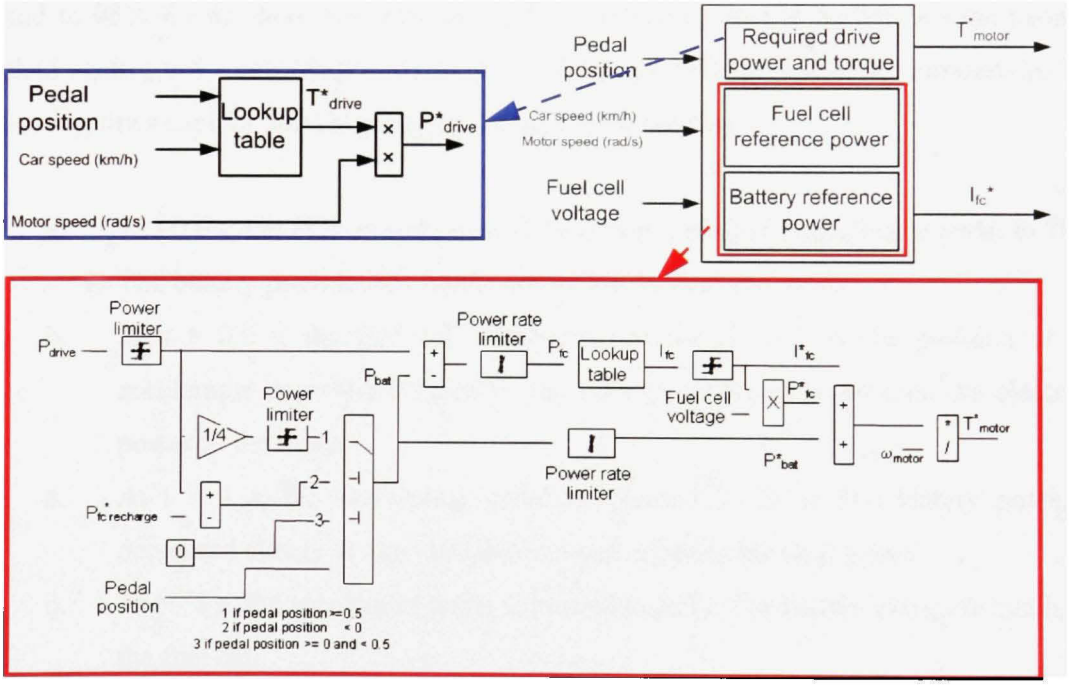

Figure 33 ***Energy management subsystem.***

The power is distributed among the electrical sources based on the position of the accelerator which varies between -100% and 100%. A negative position indicates a braking situation. When the position is less than 50%, only the fuel cell stack delivers the drive power. When it

becomes greater than 50%, the battery comes in to help the fuel cell stack. When the position is negative (regenerative braking), the motor acts as a generator and the power generated is stored in the battery which also stores the excess fuel cell power.

4.4 Simulations results and stack performance

The FCV is simulated over 14s considering different modes of operation (fast acceleration, gentle acceleration or cruising and deceleration). Figures 34 and 35 show the simulation results.

These results are obtained by maintaining the accelerator pedal constant to 70% for the first 4 s, and to 25% for the next 4 s when the pedal is released, then to 85% when the pedal is pushed again for 4 s and finally sets to -70% (braking) until the end of the simulation. The following lines explain what is going on during the simulation:

a. At t = 0 s, the FCV is stopped and the driver pushes the accelerator pedal to 70%. The battery provides the motor power till the fuel cell starts
b. At t = 0.6 s, the fuel cell begins to provide power. As the position of the accelerator is greater than 50%, the battery continues to provide the electrical power to the motor
c. At t = 4 s, the accelerator pedal is released to 25%. The battery power is decreased slowly to zero and the fuel cell supplies the total power
d. At t = 8 s, the accelerator pedal is pushed to 85%. The battery comes in and helps the fuel cell.
e. At t = 12 s, the accelerator pedal is set to -70% (regenerative braking is simulated). The motor acts as a generator driven by the vehicle's wheels. The kinetic energy of the FCV is transformed in electrical energy which is stored in the battery. For this pedal position, the required torque of -140 Nm cannot be reached because the battery can only absorb 30 kW of energy. The fuel cell power decreases to 2 kW (minimum fuel cell power) according to its response time

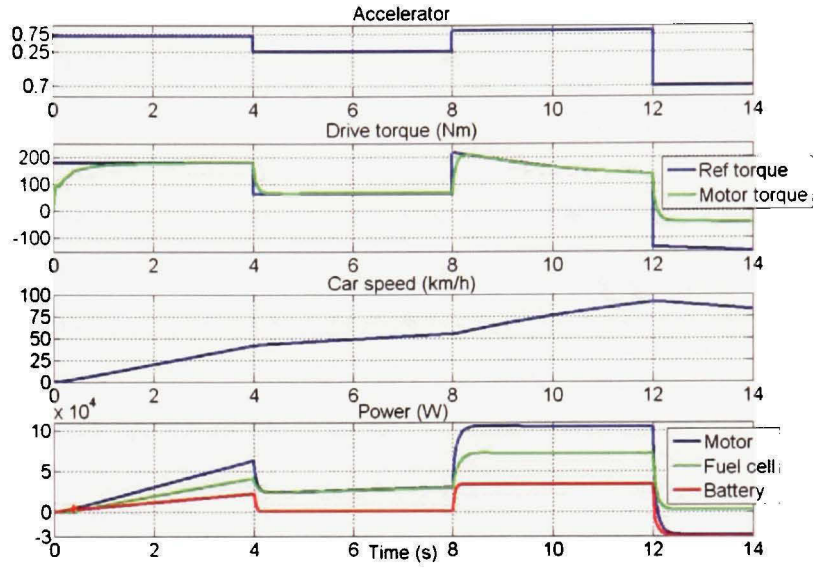

Figure 34 ***Simulation results showing the power distibution.***

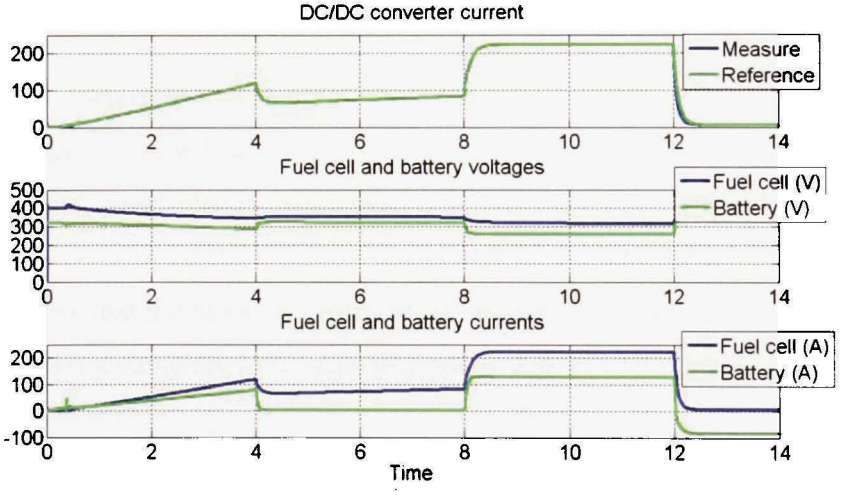

Figure 35 ***Simulation results showing the performance of the current regulator.***

It can be observed from these results that the battery is used as needed to assist the fuel cell stack and the power among these sources is distributed successfully by the energy management subsystem. The fuel cell current is well controlled by the current regulator (the fuel cell current follows exactly the reference current).

The model and the stack performance are validated by comparing the fuel consumption (mile/kg-H_2), the car acceleration and the maximum car speed with their real values obtained while driving the FCX clarity. The results obtained from the model are the following:

a. The stack consumes 175 slpm @ 100 km/h, which is 0.94 kg for 60 miles. This gives a fuel consumption of 63.82 miles/ kg-H_2
b. The car makes 0-100 km/h in 9s
c. The maximum car speed when the accelerator is 100% is 165 km/h

The real values obtained by Honda (Honda FCX Clarity Press Kit, 2008) are:

a. Fuel consumption of 68 miles/ kg-H_2
b. The car makes 0-100 km/h in 9.2s
c. The maximum speed is 160 km/h

These results prove that the model is closed to the real performance of the FCX clarity even though some model parameters were estimated due to lack of information.

The main advantages given by the proposed fuel cell stack model in this FCV demo are:

a. The inlet fuel flow rate can be adjusted such that a better fuel economy can be achieved
b. The fuel consumption and stack efficiency are readily available which allow the determination of the fuel economy and efficiency of the whole system. This feature can be very helpful in the design process of the FCV

c. The polarization curve for a given condition of operation can be determined and used to forecast the output current of the stack. This allows the control of the fuel cell power and improves greatly the energy management strategy when the stack is connected to other electrical systems.

4.5 Conclusion

In this chapter, the fuel cell stack model integrated in SPS based on the proposed models is presented. This model is used in a FCV demo to show its advantages in the simulation of fuel cell power systems and how it inter-acts with other electrical systems. The FCV has similar characteristic of the Honda FCX clarity and its subsystems are briefly described. A simulation is made over 14 s considering common modes of operation (fast acceleration, gentle acceleration or cruising, deceleration) and the results showing the power distribution and the current regulator performance are presented. The distribution of electrical energy among the battery and the fuel cell stack is found to be successfully done by the energy management subsystem. The fuel cell current is also well controlled by the DC-DC converter regulator.

The FCV model and the stack performance are validated by comparing the simulations results with true results from the FCX clarity. The two results are found to be very close even though some model parameters were estimated. The proposed fuel cell stack model offers advantages in improving the fuel economy, in estimating the efficiency of the whole system and in controlling the fuel cell power.

This FCV demo is a clear application of the proposed model and can be used as a perfect starting point on the design and simulation of any fuel cell power system.

CONCLUSION

This chapter concludes the research works performed on this project. The objective of the project was to develop a fuel cell model and to validate this model with experimental data. A generic fuel cell model is developed based on data from fuel cell stack datasheet. The user would need to extract data from the datasheet in order to perform the simulation and does not need to perform experimental test on real stack. Based on the amount of information available on a given stack, a simplified model or, alternatively, the detailed model can be used. These models are validated both with steady state V-I characteristics provided by stack manufacturers and with experimental data on a real fuel cell stack.

The V-I characteristic of a 6kW-45V fuel cell stack provided by NedStack is very close to the simulated characteristic. This same result can be obtained for any type of fuel cell.

Experimental data obtained from the EPAC-500 shows that the model has a similar behavior as the real stack when temperature, pressures and flow rates of gases change. The error between the real stack voltage and the simulated voltage is within $\pm 1\%$. This result is obtained in transient as well as in steady state and at any condition of operation, provided a controlled stack internal humidity. However, the model gives an error of 1% for every 9% increase in air pressure and an error of 3% for a 15% decrease in temperature due to the effect of humidity.

The model being validated is integrated in SPS to be available for SPS users. The integrated model is used in a fuel cell vehicle demonstration (FCV demo). This FCV demo is modeled based on the characteristic of the Honda FCX clarity developed by Honda. Even though some model parameters were estimated, the performances of the stack and the vehicle are found to be very close to their real performances in terms of fuel consumption, maximum car speed and acceleration. This confirms the validity of the FCV demo.

The fuel cell stack model proposed was found to be very helpful in improving the fuel economy, in determining the efficiency of the whole system and in controlling the fuel cell power.

The FCV demo shows how the fuel cell stack model is used with other electrical systems models and can be used as a perfect starting point in the design and simulation of fuel cell power systems.

FUTURE WORKS

Effective works have been done in this project regarding the modeling of fuel cells stack using their datasheets. With limited information provided by stack manufacturers, it is difficult to integrate the effect of parameters such as the membrane water content and porosity in the model. These parameters greatly affect the performance of the stack as they have a direct impact on the stack resistance.

An interesting follow-up research initiative could be to perform experimental tests on real fuel cells to come up with solutions to include the effect of these parameters in the model. This will improve the model performance, especially when the stack temperature greatly varies.

Another interesting research activity could be to include the possibility of supplying the fuel cell stack with alcohol (usually methanol), gasoline or any other natural gas. This can be done by developing models of fuel processor systems (reformers, burners, heaters, desulphurisers) or by considering the chemical reactions and thermodynamics principles associated with these fuel sources in the present model. The later solution will improve the model and enable the simulation of direct methanol fuel cells (DMFC) widely used in Laptops, cellular phones and PDAs. Examples of DMFC Laptops are available at TOSHIBA (http://www.toshiba.co.jp/about/press/2003_03/pr0501.htm).

APPENDIX A

SIMULINK MODELS IN SPS

A.1 Simplified model

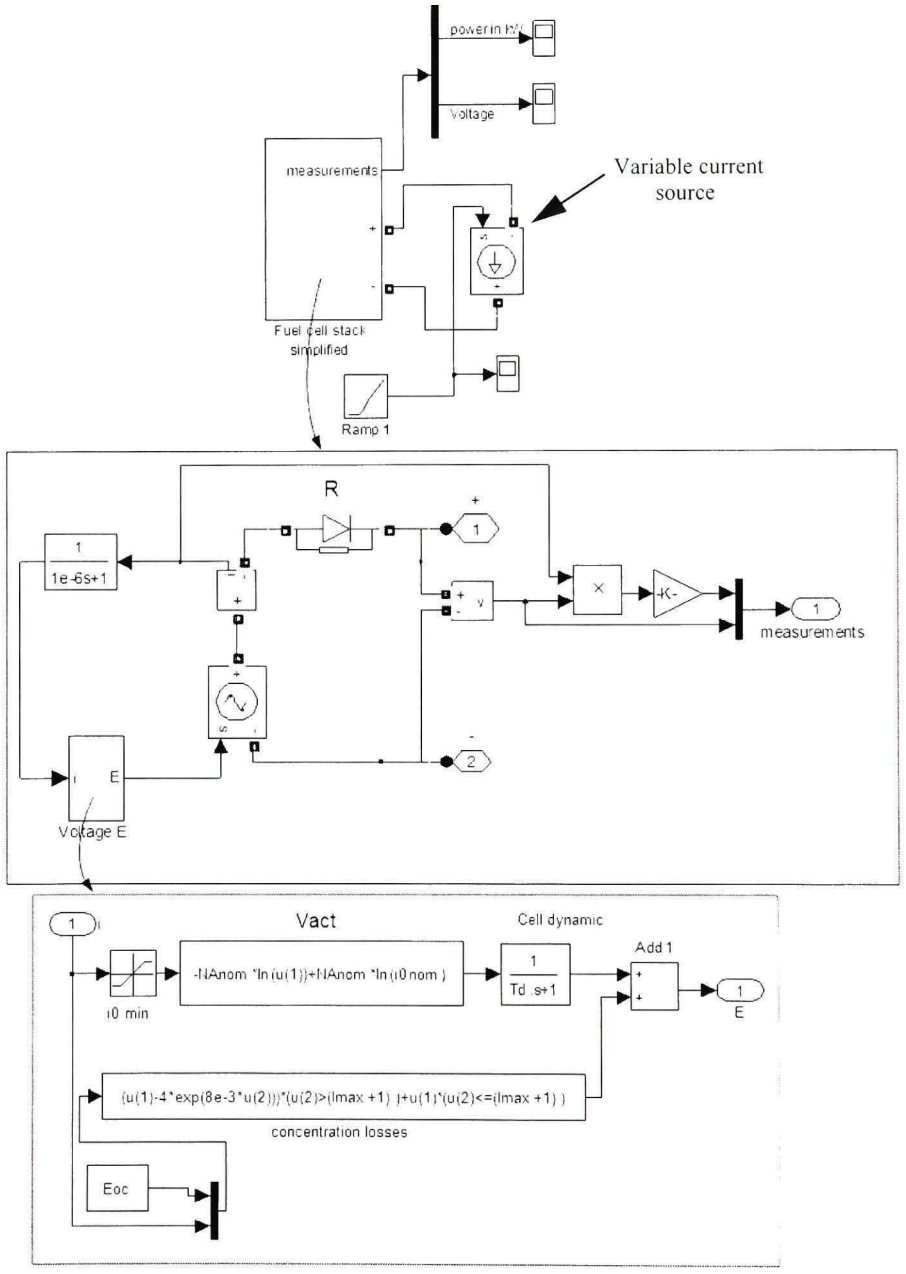

Figure 36 ***SPS simplified model (Simulink).***

A.2 Detailed model

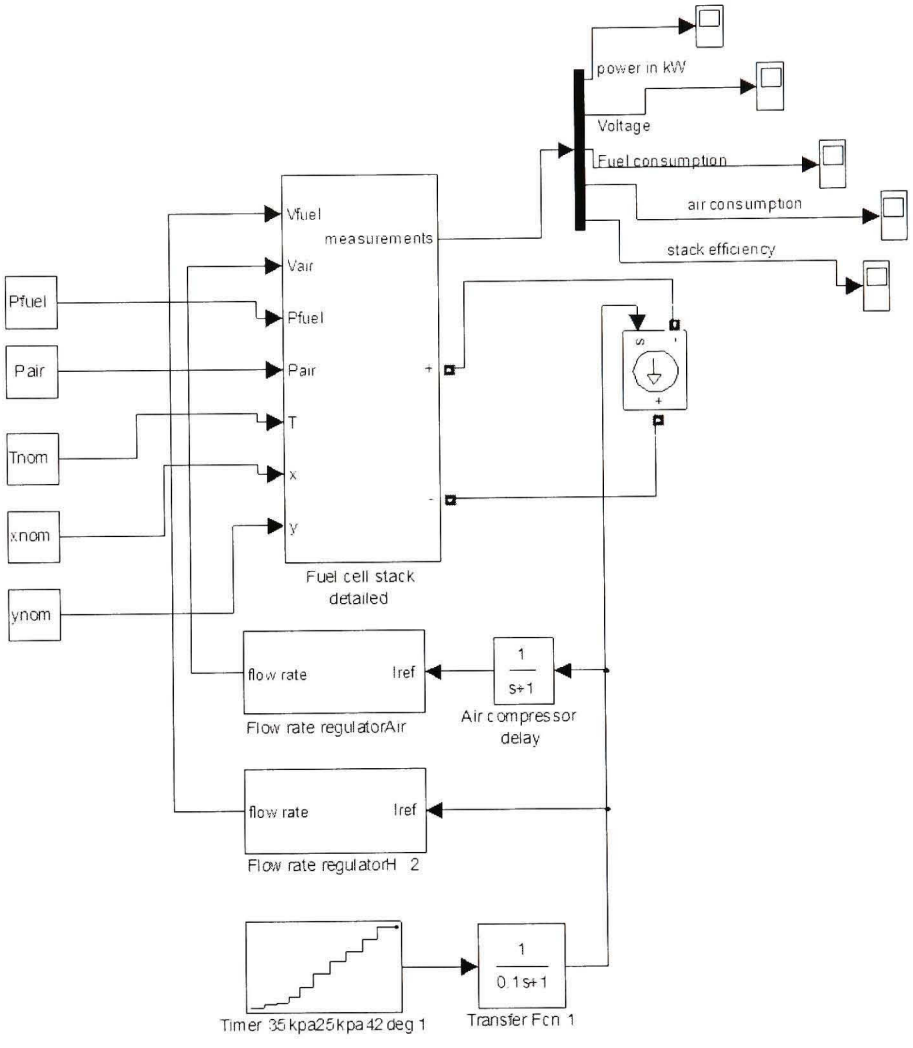

Figure 37 *SPS detailed model (Simulink).*

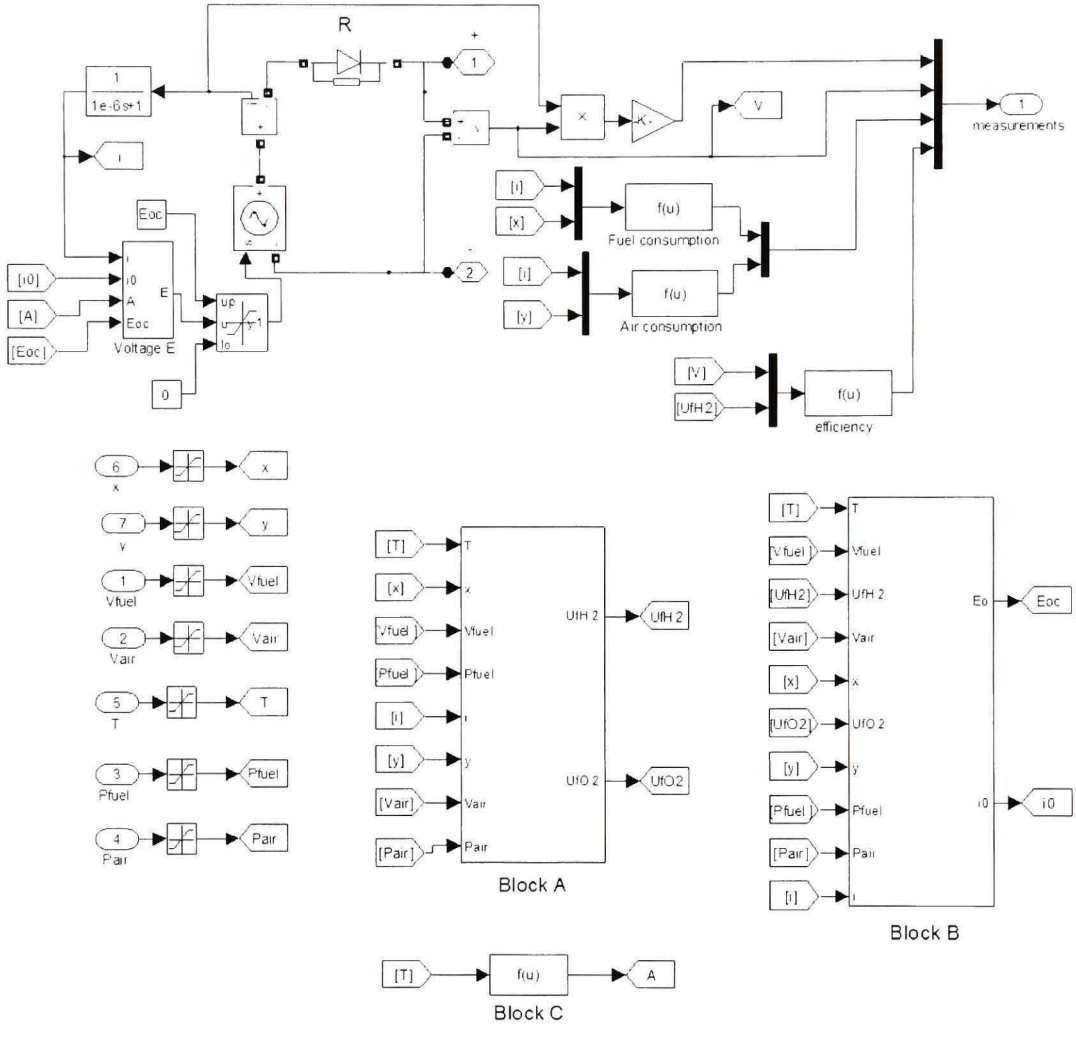

Figure 38 ***Fuel cell stack detailed (Simulink)***.

APPENDIX B

PARAMETERS EXTRACTION PROCEDURE

B.1 Stack datasheet

Type	6 kW fuel cell system	NedStack PS6
Performance	Net Rated Electrical Peak Power	7 kW (DC)
	Net Rated Electrical Nominal Power	5 kW (AC)
	Output voltage	60 – 32 V (DC)
	Operating current range	0 – 225 A (DC)
	Typical Beginning of Life Voltage Range	42 V at nominal
	Efficiency – LHV	55 % (stack) / 50 % (system)
	Time from off mode/ to idle	Within 3 min
	Time from 10% to full power	Approx. 10 s
	Expected Life	20 000 h (stack)
	Maintenance routine	2 000 h (system)
	Operational ambient temperature	-20 – +40 °C
Fuel	H2 or Reformat	
	Purity	99.999 % H2 or Reformat (<50 ppm CO)
	Supply pressure	0.5 – 5 bar
	Stack Operating Pressure	ambient
	Maximum Consumption	12.5 slpm/kW
Air delivery system	Flow rate	Max. 500 l/min
	Supply pressure	Ambient
Physical	Dimensions	400 x 600 x 1600 mm
	Mass	Approx. 80 kg
Emissions	Water collected	75 l/min
	NOx, SOx	0
Cooling system requirements	Heat Rejection to Coolant at Maximum Power	10 kW
	Maximum Ambient Temperature	45 °C
	PCPM Operating Temperature	65 °C
	Cooling method	Radiator Fan

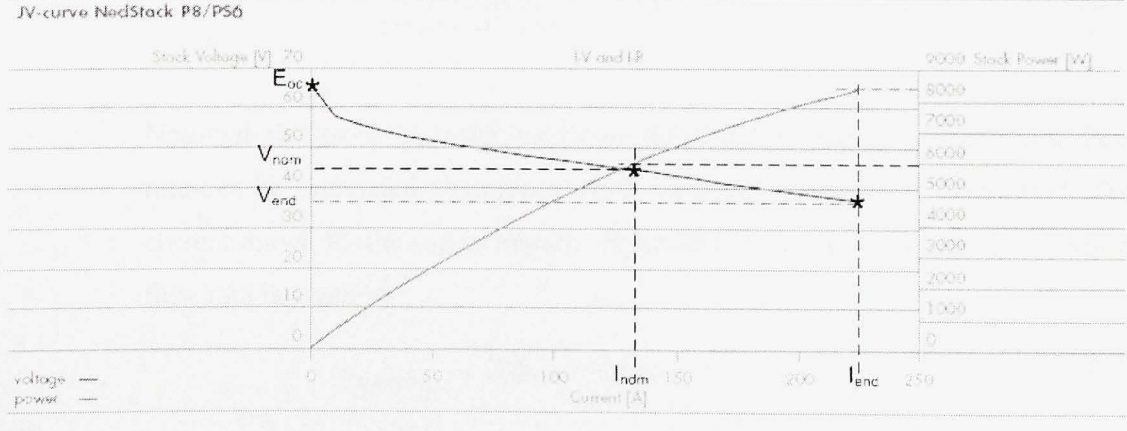

Figure 39 ***NedStack PS6 datasheet.***
(From NedStack, www.nedstack.com)

B.2 Parameters extraction

The rated power of the stack is 6 kW and the nominal voltage is 45 V. The following detailed parameters are deduced from the datasheet.

- Voltage at 0 and 1 A [E_{oc}, V_1] =[65, 64.8]
- Nominal operating point [I_{nom}, V_{nom}]=[133.3, 45]
- Maximum operating point [I_{max},V_{min}]=[225, 37]
- Nominal stack efficiency (η_{nom})= 55 %
- Operating temperature = 65 ^{0}C
- Nominal supply pressure [H_2, Air]=[1.5 1]. If the pressure given is relative to the atmospheric pressure, add 1 bar to get the absolute pressure.
- Nominal composition (%)[H_2, O_2, H_2O(Air)]=[99.999, 21, 1]. If air is used as oxidant, assume 21% of O_2 and 1% of H_2O in case their percentages are not specified.
- Number of cells: If not specified, estimate it from the formulae below:

$$N = \frac{2 \times 96485 \cdot V_{nom}}{241.83 \times 10^3 \cdot \eta_{nom}} \tag{B-1}$$

In this case,

$$N = \frac{2 \times 96485 \cdot 45}{241.83 \times 10^3 \cdot 0.55} = 65.28 \approx 65 \text{cells} \tag{B-2}$$

- Nominal air flow rate: If the maximum air flow rate is given, the nominal flow rate can be calculated assuming a constant oxygen utilization at any load. The current drawn by the cell is linearly dependent on air flow rate and the nominal flow rate is given by:

$$V_{lpm(air)_{nom}} = \frac{I_{nom} \times V_{lpm(air)_{max}}}{I_{end}} \tag{B-3}$$

In this case,

$$V_{lpm(air)_{nom}} = \frac{133.3 \times 500}{225} \approx 297 \text{liters/min} \tag{B-4}$$

In case no information is given, assume the rate of conversion of oxygen to be 50% (as it is usualy the case for most fuel cell stacks) and use the formulae below to determine the nominal air flow rate.

$$V_{lpm(air)_{nom}} = \frac{60000RT_{nom}NI_{nom}}{2zFP_{air_{nom}}0.5 \times 0.21} \tag{B-5}$$

- Fuel cell response time = 10s
- Voltage undershoot: This depends on variable such as the compressor delay and the rate of increase of current. These variables vary with the test bench, therefore experiments are needed to obtain the value of the voltage undershoot. As for the simulation, the user can input a value greater than zero to see the effect of compressor delay on the cell output voltage and power. This value is not required when there is no delay in the air compressor.

APPENDIX C

MATLAB FILE

```
%clear;
clc;

F=96485;R=8.3145;z=2;
Dh0 = 241.83e3;
k=1.38e-23;
h=6.626e-34;
Tstd = 273;
Pstd = 101325;
%input by the user-------------------------------------

%Voltage at 0 and 1 A
Eoc=65.7; V1=58.4;
%Nominal current and voltage
Inom=8.128; Vnom=50.28;
%Maximum current and minimum voltage
Imax=14.155; Vmin=45.707;
%Number of cells
N=65;
%Stack efficiency
nnom=58.83;
%operating temperature and pressure,nominal
Tc=42.3;
Tnom=Tc+273; Pfuel=1.35;Pair=1.25;
%air flow rate
Vairnom=14.91;
%composition of gases
xnom=0.9995; ynom=0.21; wnom=0.01;
%response time
Td=0.1;
%Voltage undershoot
Vu=3;
%-------------------------------------------------------------
% Model parameters, simplified and detailed model

NAnom=((V1-Vnom)*(Imax-1)-(V1-Vmin)*(Inom-1))/((log(In-
om)*(Imax-1))-(log(Imax)*(Inom-1)));
Rohm=(V1-Vnom-NAnom*log(Inom))/(Inom-1);
i0nom=exp((V1-Eoc+Rohm)/(NAnom));
%-------------------------------------------------------------
%Model parameters, detailed model

 Anom = NAnom /N;
 alpha = (R*Tnom)/(z*Anom*F);
 PH2in = xnom*Pfuel;
 PO2in = ynom*Pair;
 Uf_H2 = nnom*Dh0*N/(100*(z*F*Vnom))
 Uf_O2 = (60000*R*Tnom*N*Inom)/(4*F*Pair*Pstd*Vairnom*ynom)
 PH2 = xnom*(1-Uf_H2)*Pfuel
 PO2 = ynom*(1-Uf_O2)*Pair
     if Tc < 100
         PH2O = 1;
     else
         PH2O = (wnom+2*ynom*Uf_O2)*Pair;
     end
```

```
 Enomin = 1.229+(Tnom-298.15)*(-44.43/(z*F))+(R*Tnom/
(z*F))*log(PH2in*sqrt(PO2in));
 Enom = 1.229+(Tnom-298.15)*(-44.43/(z*F))+(R*Tnom/
(z*F))*log(PH2*sqrt(PO2)/PH2O);

 K1=2*F*k*(PH2*Pstd+PO2*Pstd)/(h*R);
 Dg= -R*Tnom*log(i0nom/K1);
 Ki=Eoc/Enomin
 Kc=Eoc/Enom
 K2=Vu/(Kc*(0.6-Uf_O2))
```

APPENDIX D

TEST SETUP AND EXPERIMENTAL RESULTS

D.1 Test setup

Experiments are made at Institut de recherche sur l'hydrogène (IRH) in Trois-Rivières. Figure 40 shows the test setup along with descriptions of important parts.

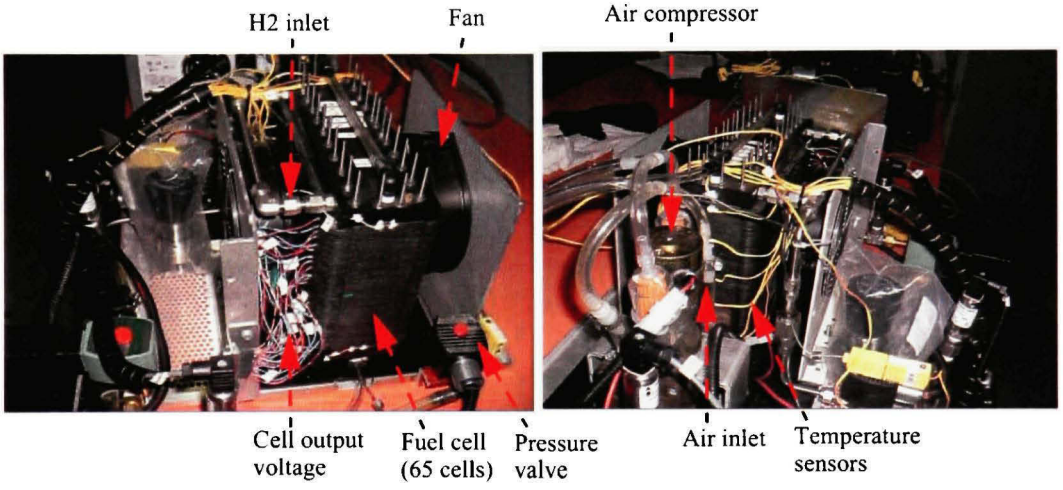

Figure 40 ***Test setup.***
(From IRH, 2008)

Source: Institut de recherche sur l'hydrogène (IRH), Trois-Rivières

The hydrogene pressure is set by the user using the pressure valve and the other parameters (air pressure, air flow rate, air utilization, load current or power) are set via the LabVIEW mask shown in figure 41.

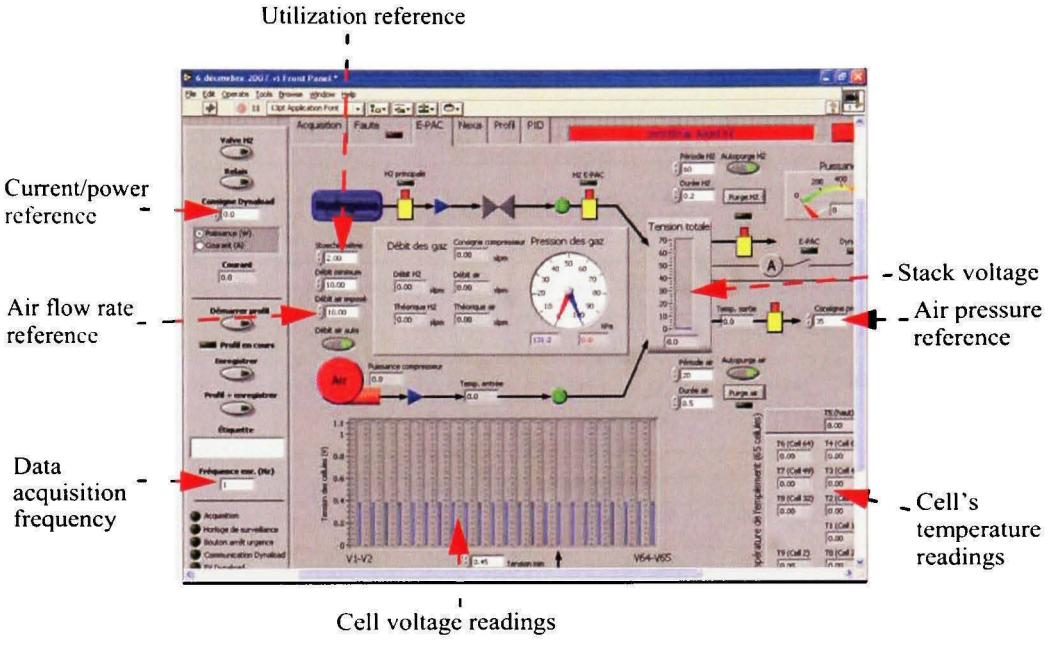

Figure 41 ***LabVIEW mask.***
(From IRH, 2008)

Source: Institut de recherche sur l'hydrogène (IRH), Trois-Rivières

D.2 Experimental results

D.2.1 Variation of inlet pressures of gases at constant stack temperature

Figure 42, 43 and 44 show the test results for different sets of inlet pressures.

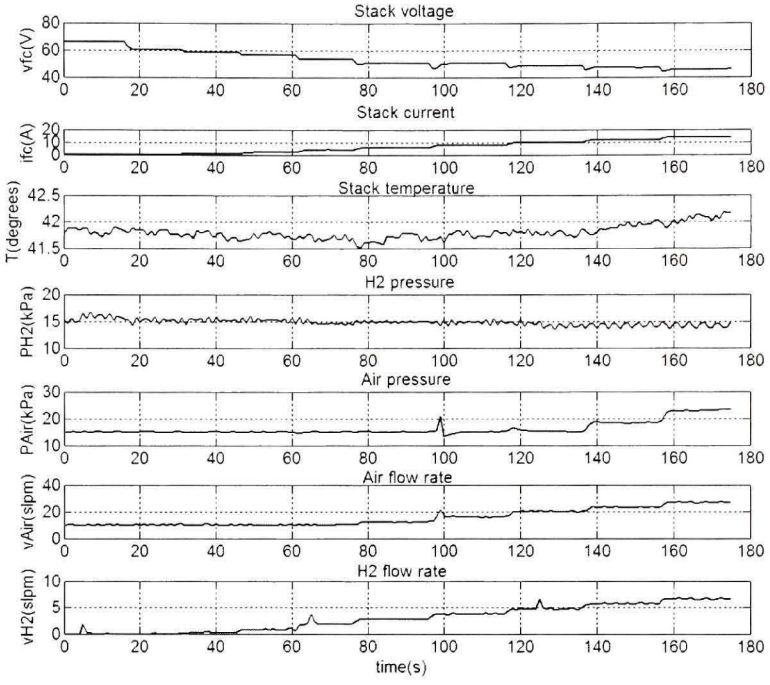

Figure 42 *Test results at P_{Air} = 15 kPa, P_{H2} = 15 kPa, T= 42 ^{o}C.*

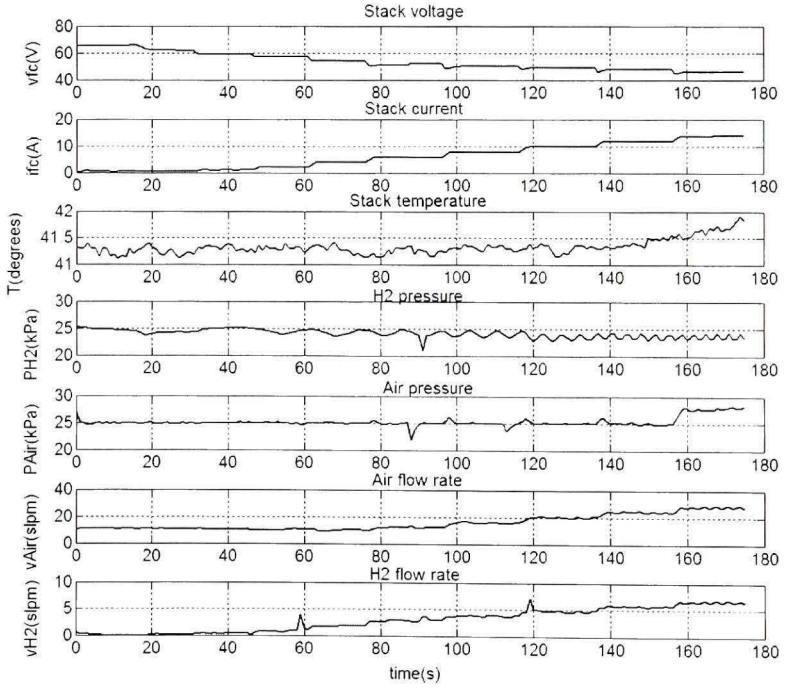

Figure 43 *Test results at P_{Air} 25 kPa, P_{H2} = 23.5 kPa, T= 42 ^{o}C.*

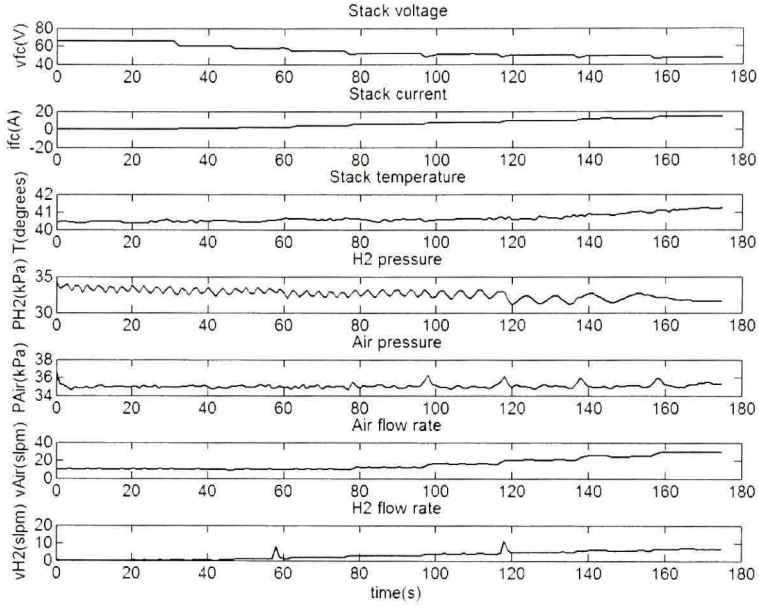

Figure 44 *Test results at P_{Air} = 35 kPa, P_{H2} = 33kPa, T= 42 ^{o}C.*

D.2.2 Variation of stack temperature at constant inlet pressures

Figure 45, 46 and 47 show the test results for different stack temperatures.

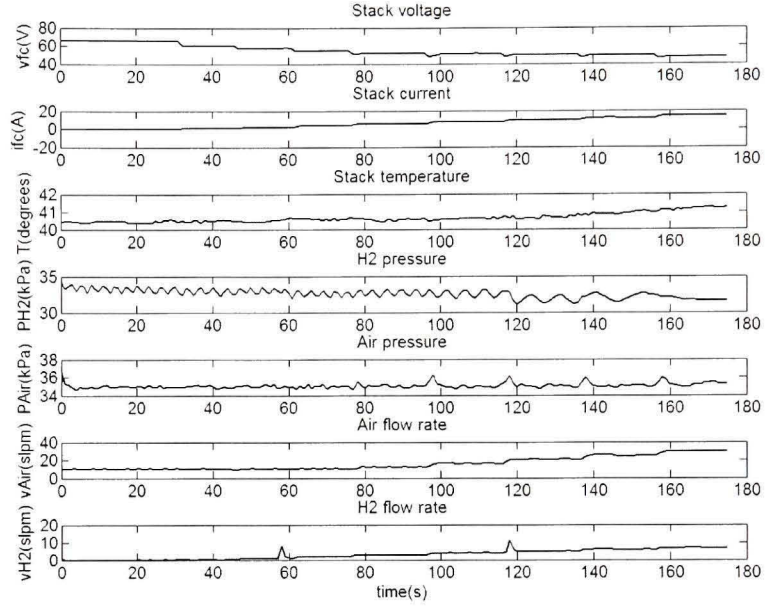

Figure 45 *Test results at P_{Air} = 35 kPa, P_{H2} = 35 kPa, T= 35°C.*

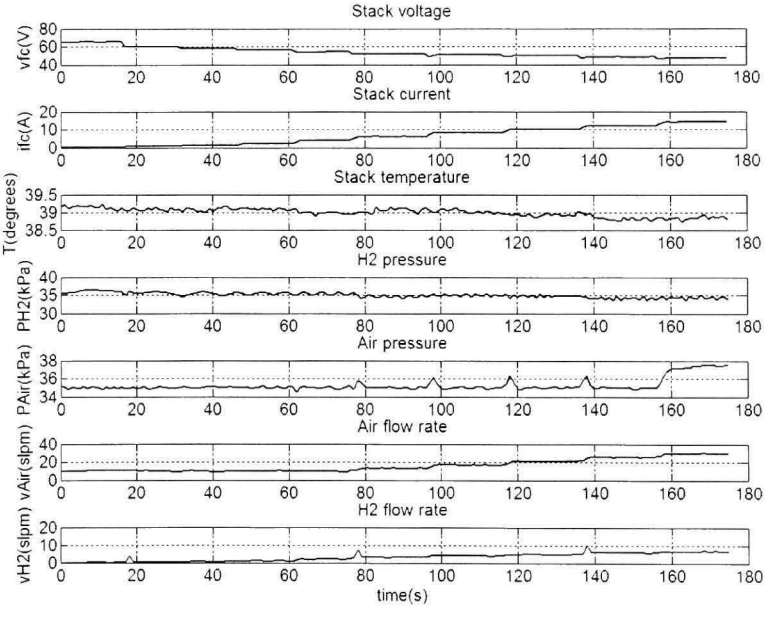

Figure 46 *Test results at P_{Air} = 35 kPa, P_{H2} = 35 kPa, T= 39°C.*

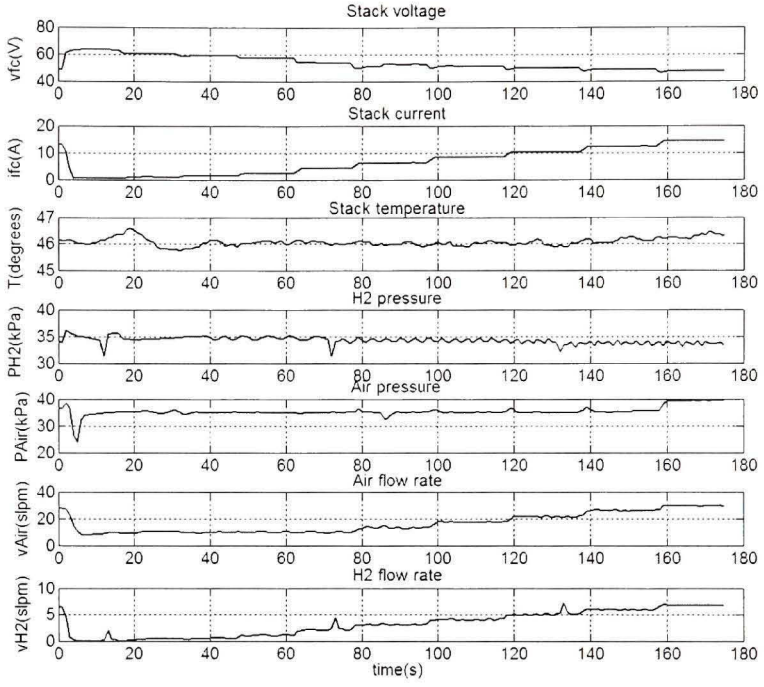

Figure 47 ***Test results at P_{Air} = 35 kPa, P_{H2} = 35 kPa, T= 46 ^{o}C.***

D.2.3 Variation of inlet air flow rate

Figure 48 and 49 show the test results for different air flow rates.

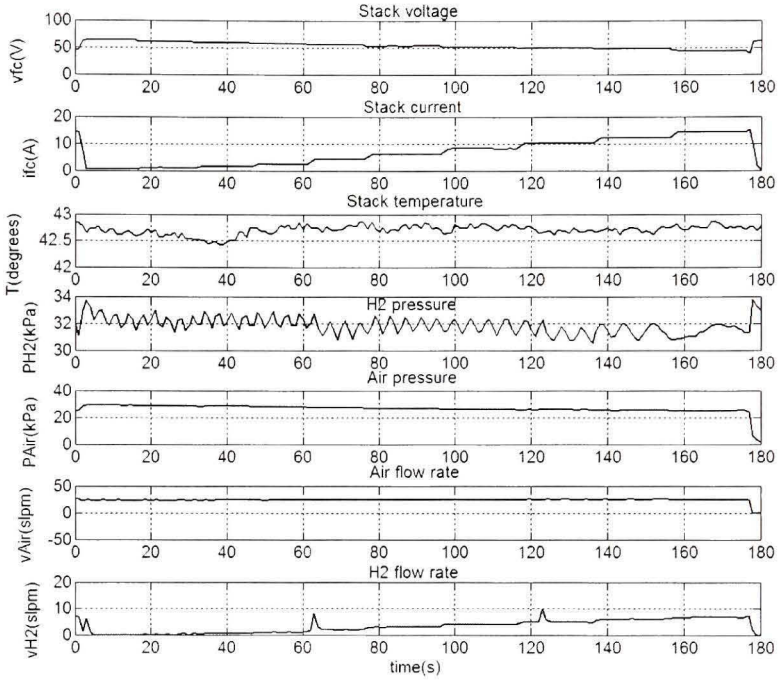

Figure 48 *Test results , V_{Air} = 25 slpm.*

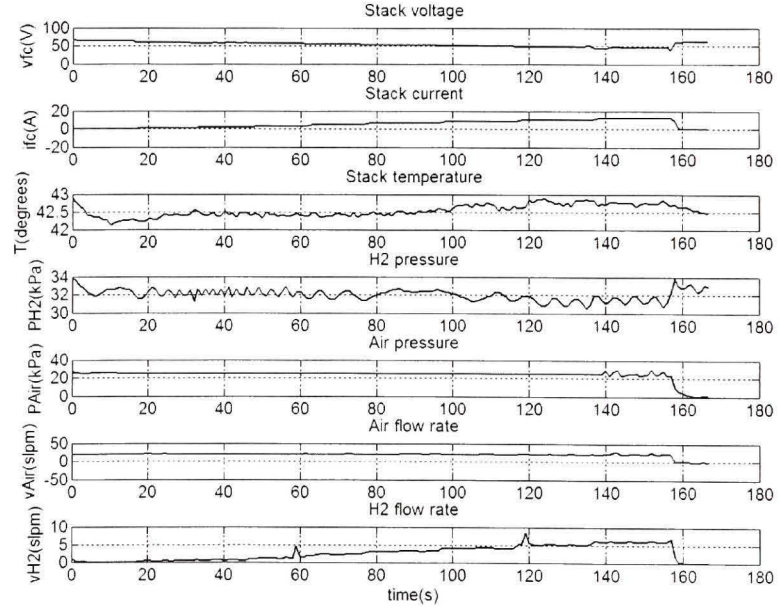

Figure 49 *Test results , V_{Air} = 20 slpm.*

BIBLIOGRAPHY

Acharya, Prabha, Prasad Enjeti and Ira J. Pitel. 2004. *An advanced fuel cell simulator*. IEEE Transactions, pp. 1554-1558.

Boettner, Daisie D., Gino Paganelli,Yann G. Guezennec, Giorgio Rizzoni and Michael J. Moran. 2002. *Proton exchange membrane fuel cell system model for automotive vehicle simulation and control*. Transactions of the ASME. Vol. 124.

Buchholz, M. and V.Krebs. 2007. *Dynamic modelling of a polymer electrolyte membrane fuel cell stack by nonlinear system identification*. Wiley interscience.www.fuel-cells.wiley-vch.de. pp. 392-401.

Honda FCX Clarity Press Kit, http://www.hondanews.com.

Kim, Min Joong, Huei Peng, Chan-Chiao Lin, Euthie Stamos and Doanh Tran. 2005. *Testing, modeling, and control of a fuel cell hybrid vehicle*. 2005 American Control Conference, Portland, OR, USA.

Kopasakis, George, Thomas Brinson, Sydni Credle and Ming Xu. 2006. *A theoretical solid oxide fuel cell Model for system controls and stability design*. National Aeronautics and Space Administration (NASA), Glenn Research Center Cleveland, Ohio 44135.

Larminie, James and Andrew Dicks. 2003. *Fuel cell systems explained*. 2nd ed. John Wiley and Sons Ltd.

Liu, Hongtan and Tianhong Zhou. 2003. *CFD based PEM fuel cell models and applications*. Nanotech 2003, vol 3, pp. 463- 466.

O'Hayre, Ryan, Suk-Won Cha, Witney Colella and Fritz B. Prinz. 2006. *Fuel cell fundamentals*. John Wiley and Sons, New York.

Pasricha, Sandip, Marc Keppler, Steven R. Shaw and M. Hashem Nehrir. 2007. *Comparison and identification of static electrical terminal fuel cell models*. IEEE Transactions, pp. 746-754.

Pukrushpan, Jay T., Anna G. Stefanopoulou, Huei peng. 2004. *Control of fuel cell power systems*. Springer-Verlag, London Limited.

Runtz, K. J. and M. D. Lyster. 2005. *Fuel cell equivalent circuit models for passive mode testing and dynamic mode design*. IEEE Transactions, pp. 794-797.

Sedghisigarchi, Kourosh and Ali Feliachi. 2004. *Dynamic and transient analysis of power distribution systems with fuel cells-Part I: Fuel-cell dynamic model*. IEEE Transactions, pp. 423- 428.

Tirnovan, R., A. Miraoui, R. Munteanu, I. Vadan and H. Balan. 2006. *Polymer electrolyte fuel cell system (PEFC) performance analysis*. IEEE Transactions.

Uzunoglu, M. and M. S. Alam. 2006. *Dynamic modeling, design, and simulation of a combined PEM fuel cell and ultracapacitor system for stand-alone residential applications*. IEEE Transactions, pp. 767- 775.

Wang, Caisheng , M. Hashem Nehrir and Steven R. Shaw. 2005. *Dynamic models and model Validation for PEM fuel cells using electrical circuits*. IEEE Transactions, pp. 442-451.

Wingelaar, P.J.H., J.L. Duarte and M.A.M. Hendrix. 2005. *Dynamic characteristics of PEM fuel cells*. IEEE Transactions, pp. 1635-1641.

Xin, Kong and Ashwin M. Khambadkone. 2003. *Dynamic modelling of fuel cell with power electronic, current and performance analysis*. IEEE Transactions, pp. 607 - 612.

Xin, Kong, Ashwin M. Khambadkone and Soy Kee Thum. 2005. *A hybrid model with combined steady state and dynamic characteristics of PEMFC fuel cell stack*. IEEE Transactions, pp. 1618 - 1625.

Yu, Qiuli, Anurag K Srivastava, Song-Yul Choe and Wenzhong Gao. 2006. *Improved modeling and control of a PEM fuel cell power system for vehicles*. IEEE Transactions, pp. 331- 336.

Zhu,Y. and K. Tomsovic. 2002. *Development of models for analyzing the load-following performance of microturbines and fuel cells*. Electric Power Systems Research 62 (2002) 1/11, www.elsevier.com/locate/epsr.